US008082107B2

US 8,082,107 B2

(12) **United States Patent**
Higginbotham et al.

(10) **Patent No.:** **US 8,082,107 B2**
(45) **Date of Patent:** ***Dec. 20, 2011**

(54) **METHODS AND COMPUTER-READABLE MEDIUM TO IMPLEMENT COMPUTING THE PROPAGATION VELOCITY OF SEISMIC WAVES**

(75) Inventors: **Joseph H. Higginbotham**, Katy, TX (US); **Morgan P. Brown**, Mountain View, CA (US)

(73) Assignee: **Wave Imaging Technology Inc.**, Houston, TX (US)

(*) Notice: Subject to any disclaimer, the term of this patent is extended or adjusted under 35 U.S.C. 154(b) by 684 days.

This patent is subject to a terminal disclaimer.

(21) Appl. No.: **12/221,390**

(22) Filed: **Aug. 1, 2008**

(65) **Prior Publication Data**

US 2010/0030479 A1 Feb. 4, 2010

(51) **Int. Cl.**
G01V 1/00 (2006.01)
G01V 1/28 (2006.01)
(52) **U.S. Cl.** **702/18**
(58) **Field of Classification Search** 702/18
See application file for complete search history.

(56) **References Cited**

U.S. PATENT DOCUMENTS

5,579,281 A	11/1996	Audebert	
5,640,368 A	6/1997	Krebs	
6,493,634 B1 *	12/2002	Krebs et al.	702/14
6,546,339 B2	4/2003	Bevc et al.	
2006/0203613 A1 *	9/2006	Thomsen et al.	367/38
2007/0263487 A1	11/2007	Jiao et al.	
2010/0114494 A1 *	5/2010	Higginbotham et al.	702/16

OTHER PUBLICATIONS

Sava et al., "Time-shift imaging condition in seismic migration", Nov.-Dec. 2006, Geophysics, vol. 71, No. 6, pp. S209-S217.*
Francois Audebert et al., Migrated focus panels: focusing analysis reconciled with prestack depth migration, SEG Expanded Abstracts, 1992, pp. 961-964.
Biondo Biondi, 3D Seismic Imaging, 2006, SEG, Tulsa, OK USA.
Jon F. Claerbout, Imaging the Earth's Interior, Blackwell Scientific Publishing, Inc., Palo Alto, CA USA. 1984.
Jon F. Claerbout, Toward a unified theory of reflector mapping, Geophysics, 1971, v. 36, pp. 467-481.
Robert G. Clapp et al., Incorporating geologic information into reflection tomography, Geophysics, 2004, v. 69, pp. 533-546.
Robert G. Clapp et al., Interval velocity estimation in a null-space, Stanford Exploration Project Report #97, pp. 147-156, Stanford, CA USA. Jul. 1998.
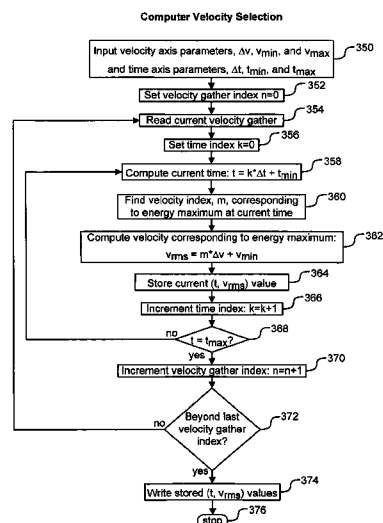
(Continued)

Primary Examiner — Michael Nghiem
(74) *Attorney, Agent, or Firm* — Robert Moll

(57) **ABSTRACT**

The invention relates to methods and computer-readable medium for computing the propagation velocity of seismic waves in the earth. The invention computes the true propagation velocity of seismic waves in the earth, which is a condition of obtaining an accurate image of subsurface geology that can be used to prospect for oil and gas deposits. In an embodiment, the method of computing the propagation velocity of seismic waves in earth, includes providing an estimate of the propagation velocity, generating a time shift gather using a depth migration at a plurality of locations of the earth, converting each of the time shift gathers to a semblance gather, transforming each semblance gather into a velocity gather whose energy peaks represent a root-mean-square average of the propagation velocity along the forward and backward path between earth's surface and a point of the subsurface geology, and converting the energy peaks to the propagation velocity.

41 Claims, 18 Drawing Sheets

Computer Velocity Selection

Input velocity axis parameters, Δv, v_{min}, and v_{max} and time axis parameters, Δt, t_{min}, and t_{max} — 350

Set velocity gather index n=0 — 352

Read current velocity gather — 354

Set time index k=0 — 356

Compute current time: $t = k^*\Delta t + t_{min}$ — 358

Find velocity index, m, corresponding to energy maximum at current time — 360

Compute velocity corresponding to energy maximum: $v_{rms} = m^*\Delta v + v_{min}$ — 362

Store current (t, v_{rms}) value — 364

Increment time index: k=k+1 — 366

$t = t_{max}$? — 368 — no / yes

Increment velocity gather index: n=n+1 — 370

Beyond last velocity gather index? — 372 — no / yes

Write stored (t, v_{rms}) values — 374

stop — 376

OTHER PUBLICATIONS

Robert G. Clapp, Geologically constrained migration velocity analysis, Ph.D. Thesis, 2001, Stanford University, Stanford, CA USA.

C.Hewitt Dix, Seismic velocities from surface measurements, Geophysics, 1955, v. 20, pp. 68-86.

Jean-Pierre Faye and Jean-Paul Jeannot, Prestack migration velocities from focusing depth analysis, SEG Expanded Abstracts, 1986, pp. 438-441.

Jeno Gazdag, et al., Migration of seismic data by phase-shift plus interpolation, Geophysics, 1984, v. 49, pp. 124-131.

Joseph H. Higginbotham et al., Directional depth migration, Geophysics, 1985, v. 50, pp. 1784-1789.

Joseph H. Higginbotham et al., Wave Equation Migration Velocity Focusing Analysis, SEG Expanded Abstracts, 2008, pp. 438-441.

Franklyn K. Levin, Apparent velocity from dipping interface reflections, Geophysics, 1971, v. 36, pp. 510-516.

Scott MacKay and Ray Abma, Imaging and velocity estimation with depth-focusing analysis, Geophysics, 1992, v. 57, pp. 1608-1622.

Tamas Nemeth, Relating depth-focusing analysis to migration velocity analysis, SEG Expanded Abstracts, 1996, pp. 463-467.

Marie L. Prucha et al., Angle-domain common image gathers by wave-equation migration, SEG Expanded Abstracts, 1999, pp.

Paul Sava and Sergey Fomel, Time-shift imaging condition in seismic migration, Geophysics, 2006, v. 71, pp. 209-217.

Paul C. Sava and Sergey Fomel, Angle-domain common-image gathers by wavefield continuation methods, Geophysics, 2003, v. 68, pp. 1065-1074.

Paul C. Sava, Migration and velocity analysis by wavefield extrapolation, Ph.D. Thesis, 2004, Stanford University, Stanford, CA USA.

Peng Shen et al., Differential semblance velocity analysis by wave-equation migration, SEG Expanded Abstracts, 2003, pp. 2132-2135.

Christiaan C. Stolk et al., Kinematic artifacts in prestack depth migration, Geophysics, 2004, v. 69, pp. 562-575.

M. Turhan Taner and Fulton Koehler, Velocity spectra—digital computer derivation applications of velocity functions, Geophysics, 1969, v. 34, pp. 859-881.

Bin Wang et al., A 3D subsalt tomography based on wave-equation migration-perturbation scans, Geophysics, 2006, v. 71, pp. 1-6.
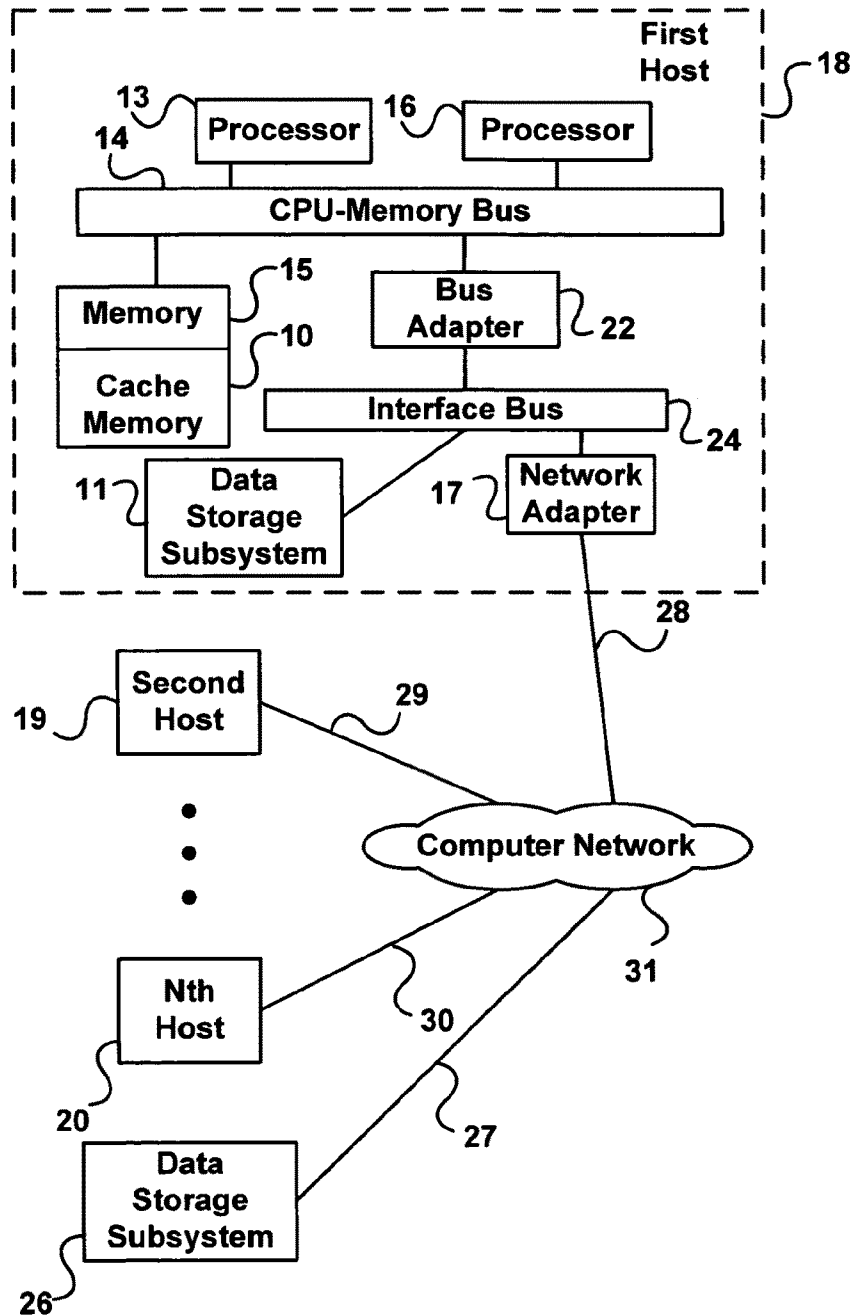
* cited by examiner

First
Host

18

13
Processor 16 Processor

14

CPU-Memory Bus

15

Memory

Bus
Adapter 22

10

Cache
Memory

Interface Bus

24

11 Data
Storage
Subsystem

17 Network
Adapter

28

Second
Host

19

29

•
•
•

Computer Network

31

Nth
Host

30

20

27

26 Data
Storage
Subsystem

FIGURE 1

Downward Continuation Migration with Correct Migration Velocity

$z = 0$

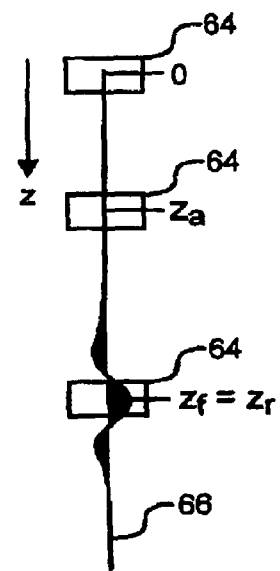s   g

z_a

z

$z_f = z_r$

(x_r, y_r, z_r)

50

FIGURE 2A

z

0   z_a $z_r = z_f$

0

t

52   54   56   58   60   62

FIGURE 2B

64

z 0

64

z_a

64

$z_f = z_r$

68
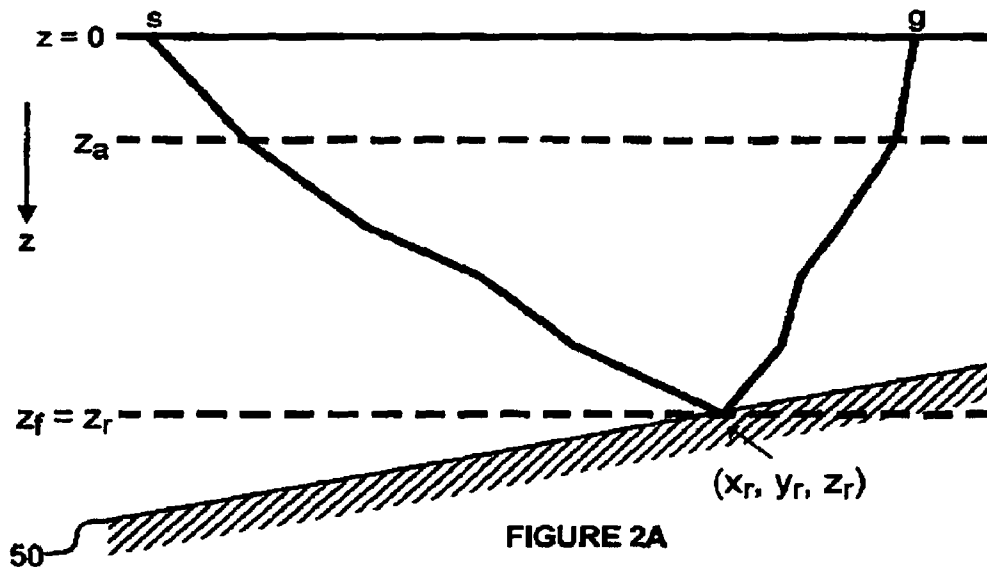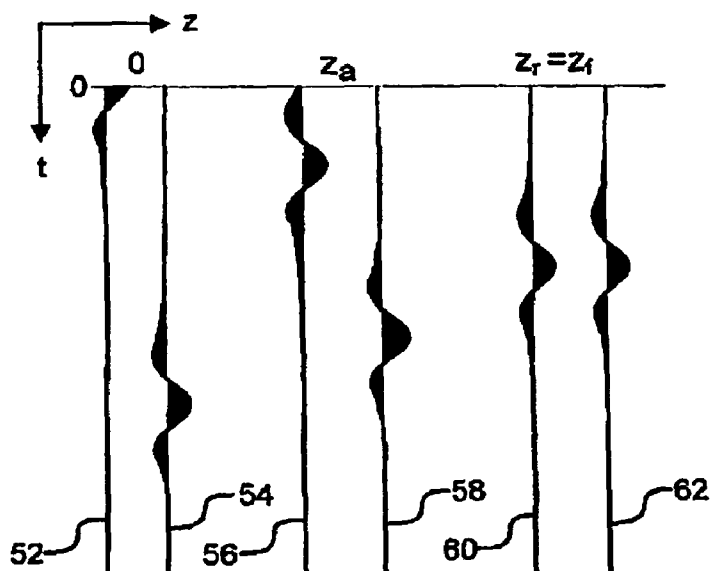
FIGURE 2C

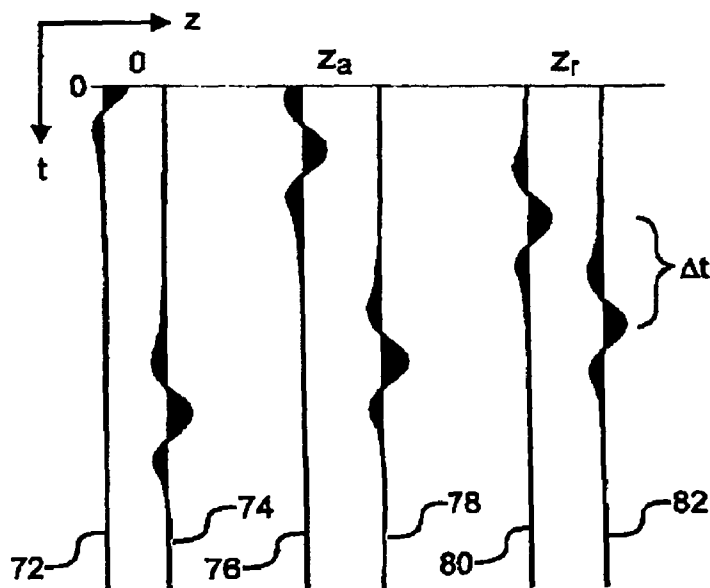**Downward Continuation Migration with Too-fast Migration Velocity**

z = 0   s   g

z_a

z

(x_r, y_r, z_r)

z_r

z_f

FIGURE 3A

50

z

0   0 z_a z_r

t

Δt

72   74   78   80   82
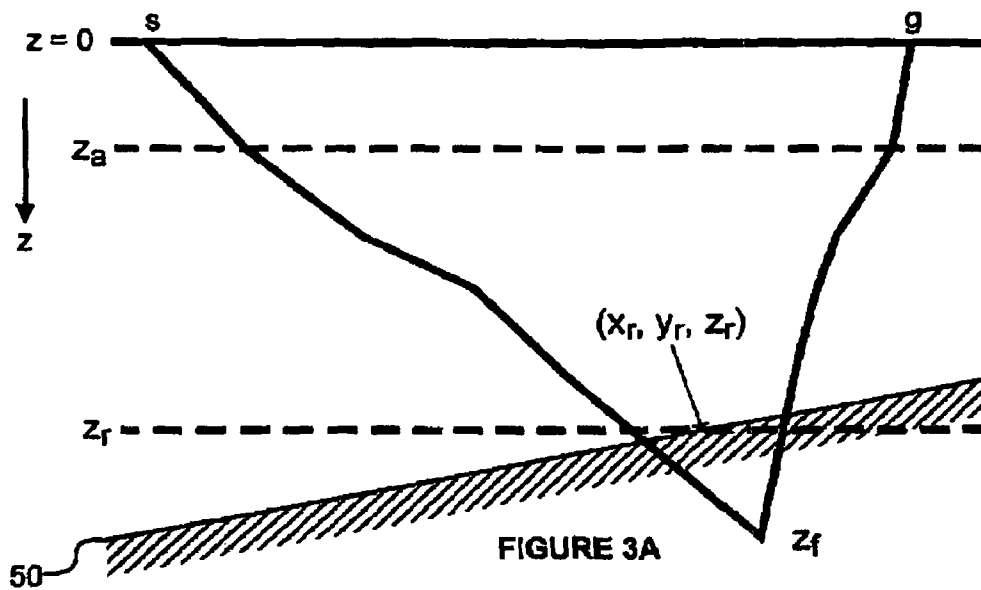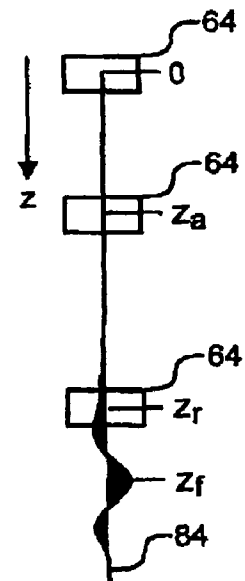
76

FIGURE 3B

64
0

z   64
z_a

64
z_r

z_f

84

FIGURE 3C

Construction of a Time-shift Gather with Too-fast Migration Velocity

FIGURE 4A

FIGURE 4B

FIGURE 4C

Survey Geometry and Shot Record Migration Image Aperture

x

y

(x_1, y_1)

(x_2, y_2)

(x_n, y_n)

$(gx_{i,1}, gy_{i,1})$

(sx_i, sy_i)

$(gx_{i,2}, gy_{i,2})$

$(gx_{i,j}, gy_{i,j})$

128

132

130

126

FIGURE 5

Downward Continuation Shot Record Migration

Input N_{shots}, axis parameters ($\Delta\omega$, ω_{min}, ω_{max}) and (Δz, z_{min}, z_{max}) ⟋138

Set frequency index j=0 ⟋140

Compute current frequency, $\omega = j\Delta\omega + \omega_{min}$ ⟋142

Set shot gather index i=0 ⟋144

Read source location (sx_i, sy_i), define shot image aperture ⟋146

Read synthetic source function frequency slice, f(ω, x, y) ⟋148

Read shot gather frequency slice, G(ω, g_x, g_y) ⟋150

Initialize source field: S = f(ω, x, y) ⟋152

Initialize receiver field: R = G(ω, x, y) ⟋154

Set depth index k=0 ⟋156

Migrate depth z=k*Δz + z_{min} ⟋158

Downward continue S to depth z + Δz ⟋160

Downward continue R to depth z + Δz ⟋162

Compute time-shift gathers at depth z + Δz → (A) FIGURE 7 ⟋164

Increment depth index: k=k+1 ⟋166

z = z_{max}? ⟋168   no / yes

Increment shot index: i=i+1 ⟋170

i = N_{shots}? ⟋172   no / yes

Increment frequency index: j=j+1 ⟋174

$\omega = \omega_{max}$? ⟋176   no / yes

Write time-shift gathers and amplitude-squared time-shift gathers ⟋178

FIGURE 6

Construction of a Collection of Time-Shift Gathers

FIGURE 6

(A)

Input receiver wave field, R(x,y), and source wave field, S(x,y), at depth z, source location (sx_i, sy_i), frequency ω

Input $\Delta\tau$, τ_{min}, τ_{max} ⌐181

180

Set time shift index: m=0

182⌐

Set time shift $\tau = m*\Delta\tau + \tau_{min}$ ⌐183

Apply time-shift imaging condition: ⌐184
For all (x,y), A(x,y) = [R(x,y) exp(i$\omega\tau$)] * [S(x,y) exp(-i$\omega\tau$)]

Set time-shift gather index n=0 ⌐185

Compute time-shift gather at location (x_n, y_n) ⌐186

(x_n, y_n) contained in image aperture of shot at (sx_i, sy_i)? ⌐187

no

yes

Add into time-shift gather: $T_n(z, \tau) = T_n(z, \tau) + A(x_n, y_n)$ ⌐188

Add into amplitude-squared time-shift gather: $Q_n(z, \tau) = Q_n(z, \tau) + A^2(x_n, y_n)$ ⌐189

Increment time-shift gather index: n=n+1 ⌐190

Beyond last time-shift gather index? ⌐192

no

yes

Increment time-shift index: m=m+1 ⌐194

$\tau = \tau_{max}$? ⌐196

no

yes

Continue with Shot Record Migration → (A) FIGURE 6

198⌐

FIGURE 7

Flattening a Time-Shift Gather

202 — Set time-shift gather index n=0

204 — Input time-shift gather location, (x_n, y_n)

206 — Read migration velocity at (x_n, y_n): $V_m(z)$

208 — Read time-shift gather: $T_n(z, \tau)$

210 — Read amplitude-squared time-shift gather: $Q_n(z, \tau)$

212 — Convert depth axis to time

214 — Convert depth axis to time

216 — Shift each trace by τ

218 — Shift each trace by τ

220 — Write retarded time-shift gather $T_n(t, \tau)$

222 — Write retarded amplitude-squared time-shift gather $Q_n(t, \tau)$

224 — Increment time-shift gather index: n=n+1

226 — Beyond last time-shift gather index?

no

yes

227 — done

FIGURE 8A

τ_{min} $\tau=0$ τ_{max}

Time-shift Gather

z

228

FIGURE 8B

τ_{min} $\tau=0$ τ_{max}

Retarded Time-shift Gather

229

t

FIGURE 8C

Count the Shots Contributing to a Time-Shift Gather

Input image aperture parameters, N_{shots} — 230

Set source index i=0 — 232

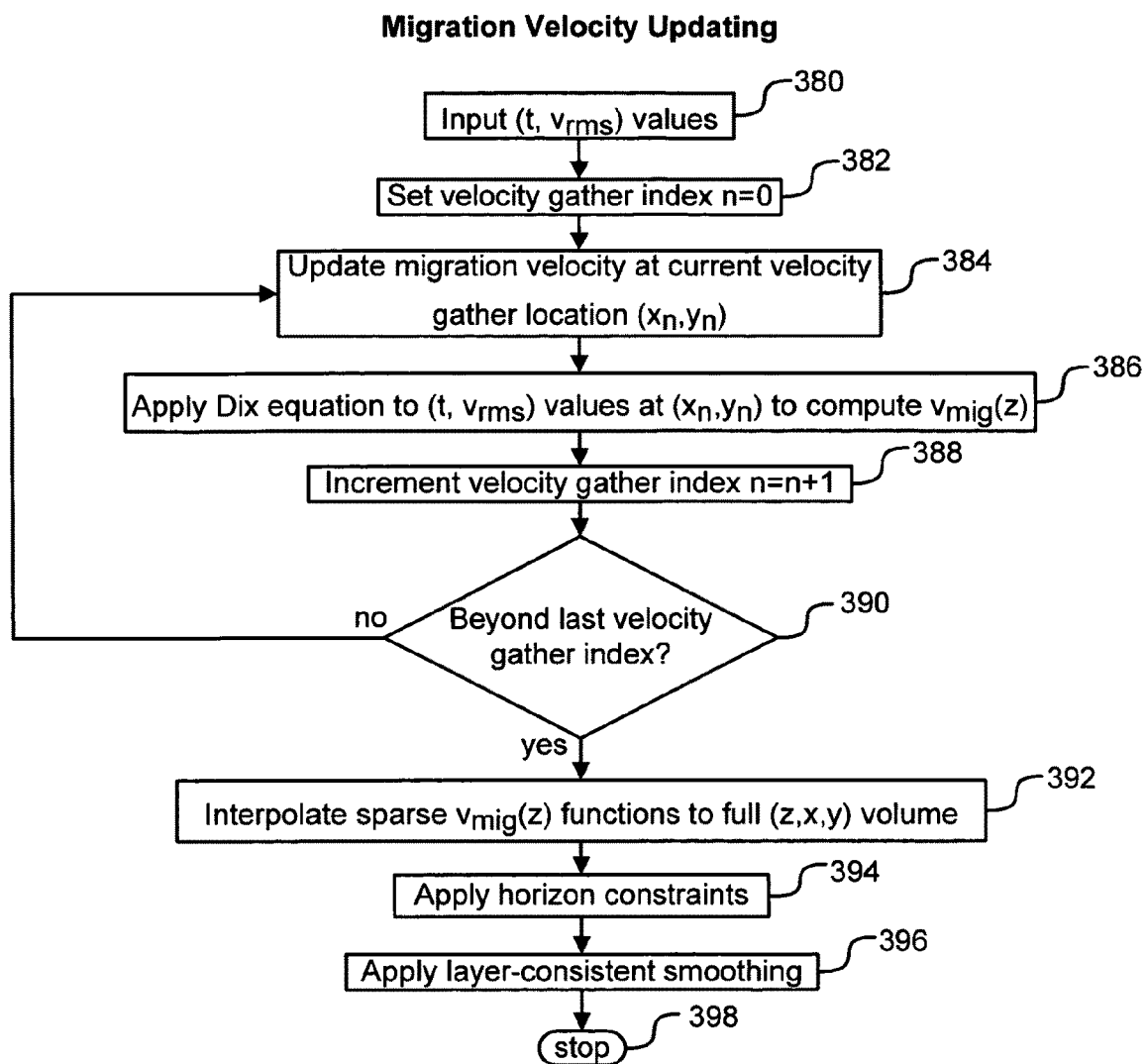Read ith source location: (sx_i, sy_i) — 234

236 — Define shot image aperture relative to (sx_i, sy_i) → (B) FIGURE 5

Set time-shift gather index n=0 — 238

Read current time-shift gather location, (x_n, y_n) — 240

no ← (x_n, y_n) contained in current shot image aperture? — 242

yes ↓

244 — Increment source count, write to header of time-shift gather

Increment time-shift gather index: n=n+1 — 246

no ← Beyond last time-shift gather index? — 248

yes ↓

Increment source index: i=i+1 — 250

no ← i > N_{shots}? — 252

yes ↓

done — 254

FIGURE 9

Semblance Computation

Set time-shift gather index n=0 ⟋262

Compute nth semblance gather ⟋264

Read retarded time-shift gather, $T_n(t,\tau)$

266⟋

Read retarded amplitude-squared time-shift gather, $Q_n(t,\tau)$ ⟋268

Read source count, N

270⟋

Compute semblance gather, $S(t,\tau)$. For each (t,τ):

$$S_n(t,\tau) = \frac{T_n(t,\tau)^2}{N \cdot Q_n(t,\tau)}$$

⟋272

Increment time-shift gather index: n=n+1 ⟋274

Beyond last time-shift gather index? ⟋276

no

yes

Write file of semblance gathers ⟋278

done ⟋280

FIGURE 10

Wave Equation Migration Velocity Focusing Analysis (MVFA)

Input velocity perturbation axis parameters, $\Delta(\Delta v)$, Δv_{min}, and Δv_{max} ⟶ 290

Set semblance gather index n=0 ⟶ 292

Read semblance gather location: (x_n, y_n) ⟶ 294

Read semblance gather, $S_n(t, \tau)$ ⟶ 295

Read migration velocity at (x_n, y_n), $V_m(z)$ ⟶ 296

300

Convert depth axis to time ⟶ 298

Select desired MVFA equation

Set velocity perturbation index j=0 ⟶ 302

Interpolate velocity perturbation: $\Delta v = j*\Delta(\Delta v) + \Delta v_{min}$ ⟶ 304

Compute τ corresponding to Δv ⟶ 306

Compute bracketing time shifts about computed τ: τ_0 and τ_1, and associated linear interpolation weights, w_0 and w_1 ⟶ 308

For each t, linearly interpolate to compute velocity gather: $M_n(t, v_m(t)+\Delta v_j) = w_0*S_n(t, \tau_0) + w_1*S_n(t, \tau_1)$ ⟶ 309

Increment velocity perturbation index: j=j+1 ⟶ 310

$\Delta v = \Delta v_{max}$? ⟶ 312

no

yes

Write current velocity gather $M_n(t, v+\Delta v)$ ⟶ 314

Increment semblance gather index: n=n+1 ⟶ 316

Beyond last semblance gather index? ⟶ 318

no

yes

done ⟶ 320

FIGURE 11

Manual Velocity Selection

Input velocity gathers to computer ⟵ 330

User chooses first velocity gather ⟵ 332

Display current velocity gather ⟵ 334

User picks set of (t, v_{rms}) values corresponding to energy maxima ⟵ 336

Beyond last velocity gather? ⟵ 338

no

yes

Write (t, v_{rms}) pick set ⟵ 339

stop ⟵ 340

FIGURE 12A

τ_{min}　0　τ_{max}　τ

Retarded Time-shift Gather

t

229

FIGURE 12B

τ_{min}　0　τ_{max}　τ

Semblance Gather

t

342

341

FIGURE 12C

v_{min}　v_{max}　v_{RMS}

Velocity Gather

t

344

349

348

346

$V_m(t)$

FIGURE 12D

Computer Velocity Selection

Input velocity axis parameters, Δv, v_{min}, and v_{max} and time axis parameters, Δt, t_{min}, and t_{max} ⟋350

Set velocity gather index n=0 ⟋352

Read current velocity gather ⟋354

Set time index k=0 ⟋356

Compute current time: $t = k^*\Delta t + t_{min}$ ⟋358

Find velocity index, m, corresponding to energy maximum at current time ⟋360

Compute velocity corresponding to energy maximum: $v_{rms} = m^*\Delta v + v_{min}$ ⟋362

Store current (t, v_{rms}) value ⟋364

Increment time index: k=k+1 ⟋366

$t = t_{max}$? ⟋368
no
yes

Increment velocity gather index: n=n+1 ⟋370

Beyond last velocity gather index? ⟋372
no
yes

Write stored (t, v_{rms}) values ⟋374

stop ⟋376

FIGURE 13

Migration Velocity Updating

Input (t, v_{rms}) values — 380

Set velocity gather index n=0 — 382

Update migration velocity at current velocity gather location (x_n, y_n) — 384

Apply Dix equation to (t, v_{rms}) values at (x_n, y_n) to compute $v_{mig}(z)$ — 386

Increment velocity gather index n=n+1 — 388

Beyond last velocity gather index? — 390

no

yes

Interpolate sparse $v_{mig}(z)$ functions to full (z,x,y) volume — 392

Apply horizon constraints — 394

Apply layer-consistent smoothing — 396

stop — 398

FIGURE 14

A Time-shift Gather

FIGURE 15

Velocity Gathers with Varying Amount of Velocity Error

RMS Velocity (m/sec)

FIGURE 16A

RMS Velocity (m/sec)

FIGURE 16B

RMS Velocity (m/sec)

FIGURE 16C

Migration Results with Varying Velocity Errors

X (m)

FIGURE 17A

X (m)

FIGURE 17B

X (m)
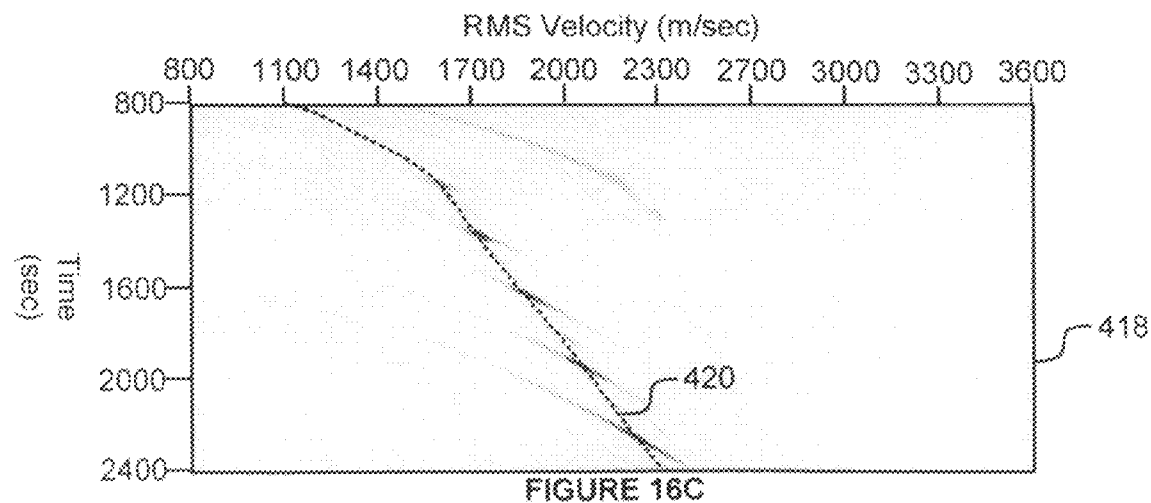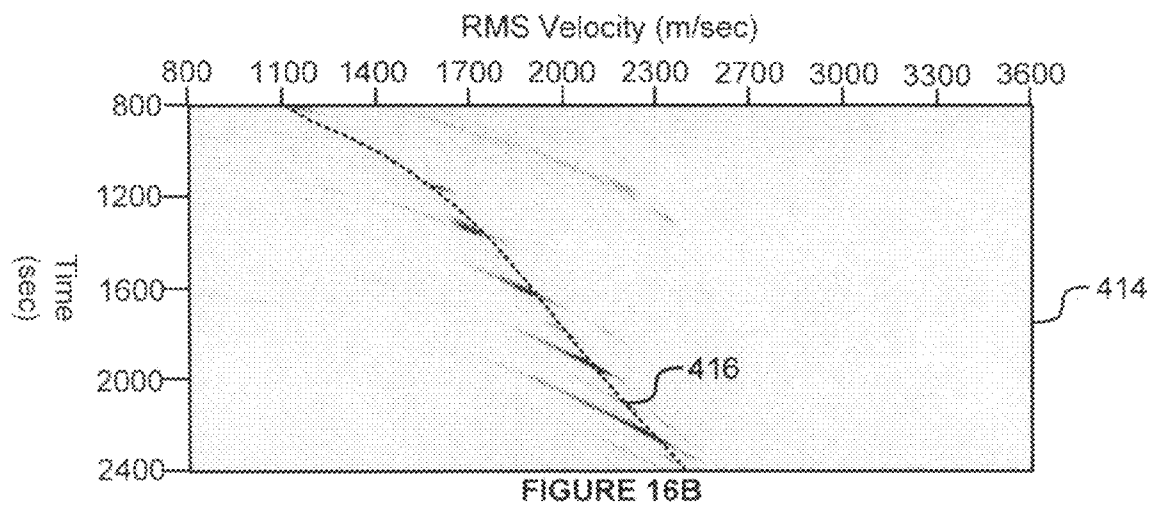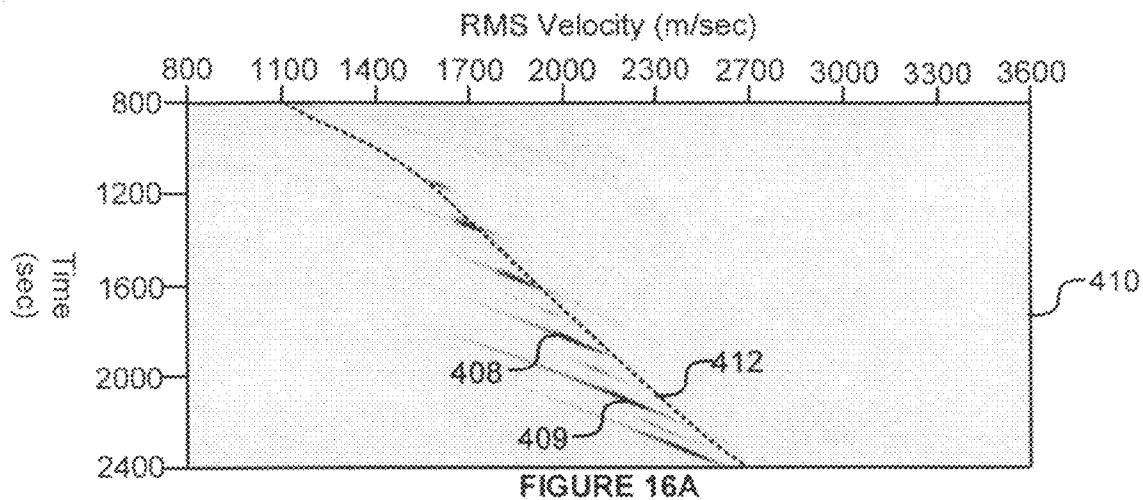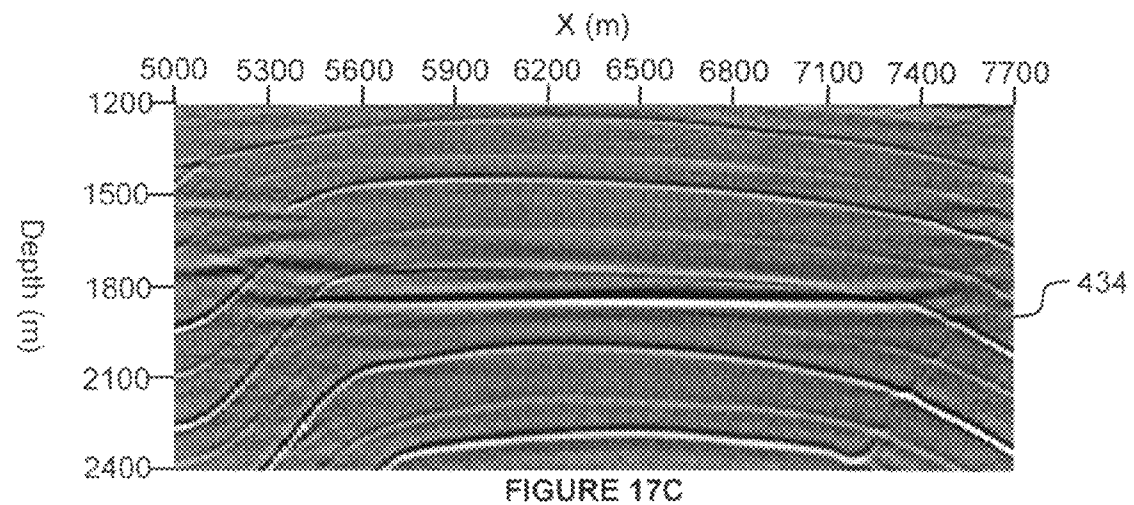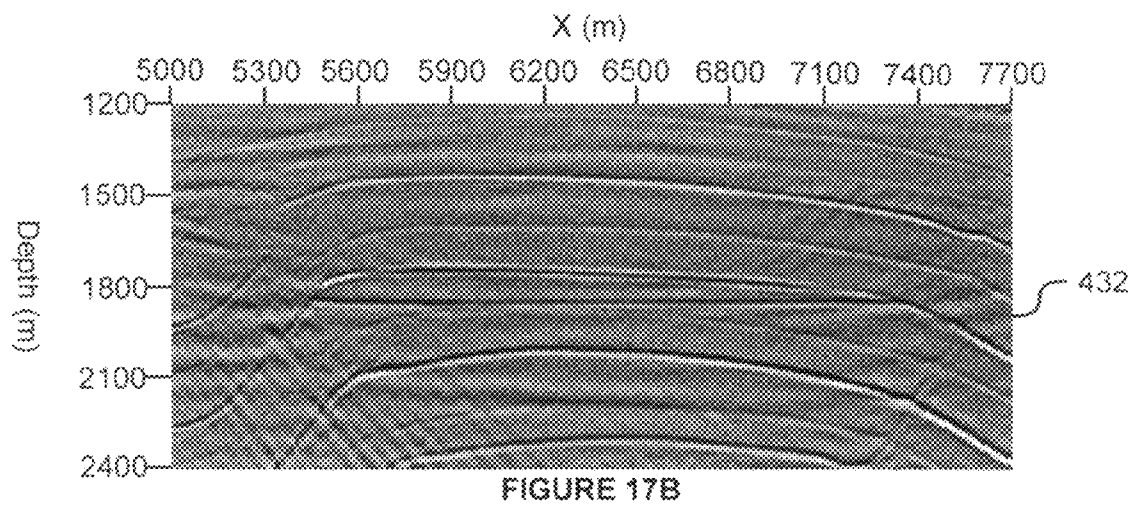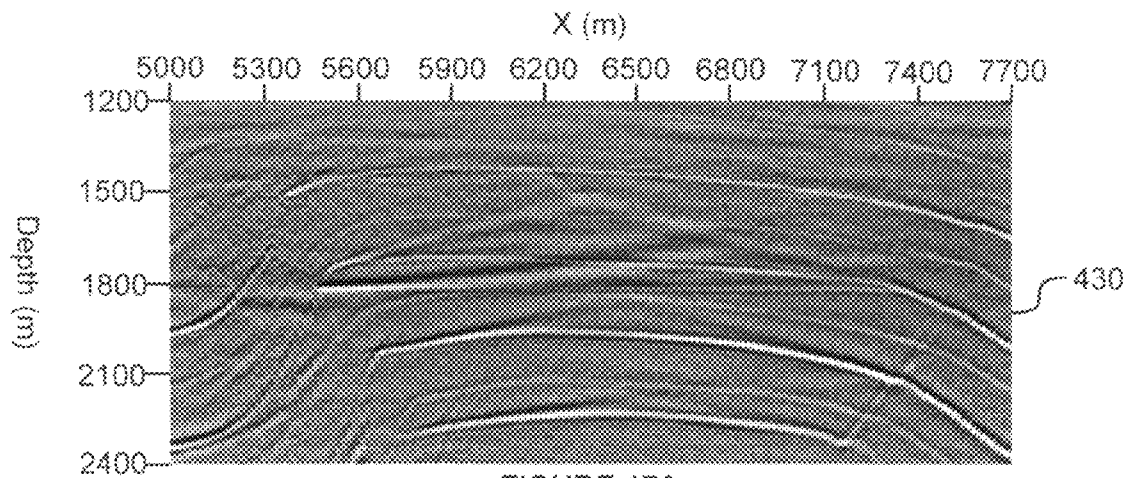
FIGURE 17C

Comparison of Velocity Models Used in Feasibility Test

X (m)

FIGURE 18A

X (m)

FIGURE 18B

X (m)
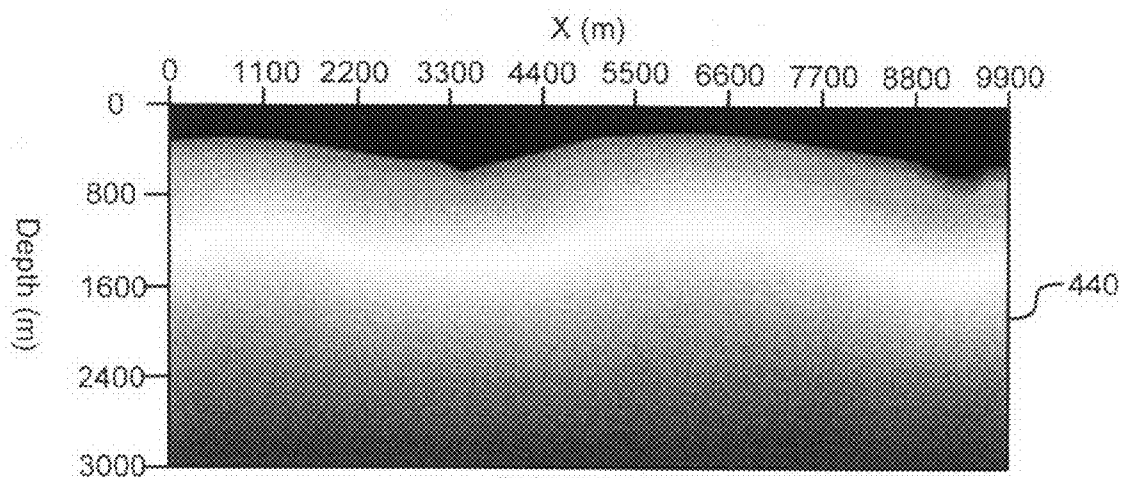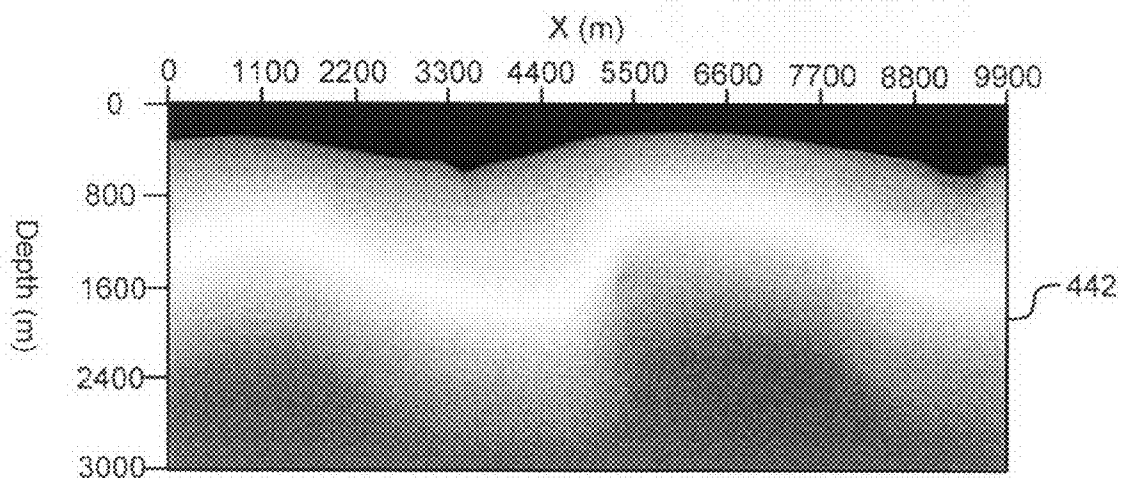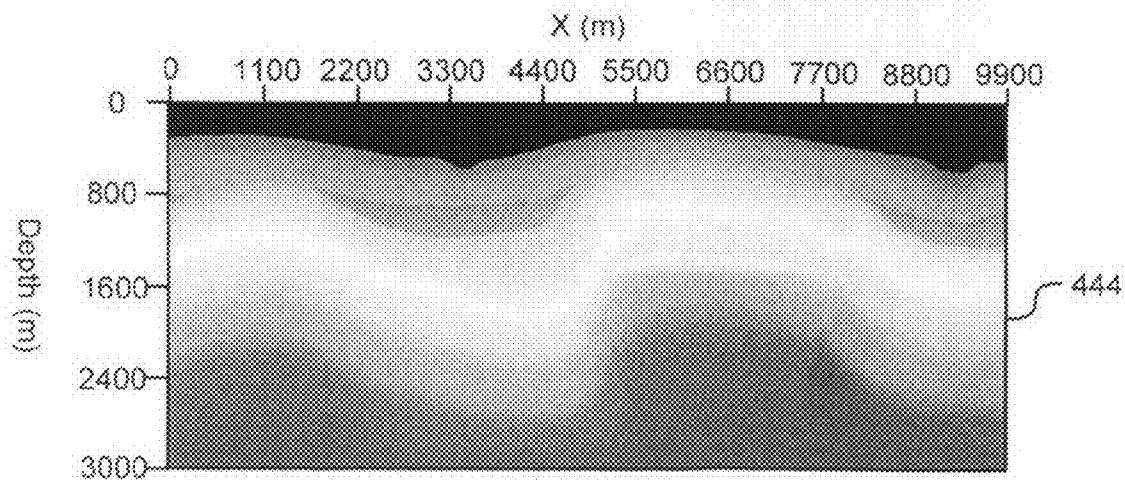
FIGURE 18C

METHODS AND COMPUTER-READABLE MEDIUM TO IMPLEMENT COMPUTING THE PROPAGATION VELOCITY OF SEISMIC WAVES

BACKGROUND

The invention relates to methods and computer-readable media to implement computation of the propagation velocity of seismic waves.

Knowledge of the propagation velocity of seismic waves is required to produce accurate images of underground geology to prospect for oil and gas with the reflection seismic method. The reflection seismic method deploys an array of sound sources (e.g., dynamite, air guns, and vibrating trucks) and receivers (e.g., seismometer or hydrophone) on or below earth's surface to construct an image of underground geology. To gather data to make the image, each sound source produces an explosion or vibration that generates seismic waves that propagate through earth, or initially through water then earth. Underground geologic interfaces, known as "reflectors," will reflect some energy from the seismic waves back to the receivers. Each receiver will record a "trace" at that time. A multi-channel seismic recording system such as the Strata-View manufactured by Geometrics Inc., San Jose, Calif. can be used to collect all of the recorded traces for a given shot. This collection is referred to as a "shot gather."

To map the underground geology, the recorded time of the shot reflection events of each seismic trace will be mapped to the position at which the reflection occurred, using the propagation velocities of seismic waves, which vary with respect to spatial position. This mapping is known as "prestack depth migration." Claerbout, *Toward a unified theory of reflector mapping*, Geophysics v. 36, p. 467 (1971), which is incorporated by reference herein, describes a method of computation known as "downward continuation," which enables prestack migration. Downward continuation is a computation that mathematically moves the recorded seismic traces and simulated seismic source traces into the subsurface to achieve prestack depth migration.

Downward continuation requires an initial estimate of propagation velocity known as the "migration velocity." These estimated propagation velocities can be obtained for instance by the method of stacking velocity analysis developed by Taner and Koehler, *Velocity spectra—digital computer derivation applications of velocity functions*, Geophysics 34, p. 859 (1969), which is incorporated by reference herein.

To form an image from the recorded data at a given depth, downward continuation migration computes the dot product of the downward continued recorded seismic trace and its corresponding downward continued source trace. When an energy peak on the recorded trace is time-coincident with an energy peak on the source trace an image can be formed. This method is known as the "zero time lag correlation imaging condition." It is noted that the term "lag" is also referred to as "shift." If the migration velocity matches the true propagation velocity, prestack migration will form an image of the reflector at the correct location. If the migration velocity differs from the true propagation velocity, prestack migration will form an image of the reflector at an incorrect location.

Sava and Fomel, *Time-shift imaging condition in seismic migration*, Geophysics, v. 71, p. 209 (2006), which is incorporated by reference, state that the zero time lag correlation imaging condition may be generalized to extract energy at a non-zero time lag and used to estimate the propagation velocities. When the migration velocity is incorrect, the

energy peak on the downward continued source trace will not match the time of the energy peak on the downward continued recorded trace. By applying the correlation imaging condition at a number of time shifts, other than at zero lag, the amount of misfocusing in time can be computed and related to a velocity error. The generalized imaging condition is known as the "time-shift imaging condition." For a given position on the recording surface and a given time shift, all the traces are summed. The collection of all these summed traces at that position for all the time shifts is known as "a time-shift gather."

In regions with significant geologic complexity, velocity analysis using depth migration (MVA) is superior to methods which operate on prestack data. Migration in general, and depth migration in particular, simplify prestack data by correcting for the effects of offset, reflector dip, and propagation from source to receiver in a heterogeneous medium. When the migration velocity is incorrect, migration will incorrectly position the surface data in depth. Some MVA techniques attempt to flatten Kirchhoff common-offset depth migration gathers by measuring depth error as a function of offset and perturbing the migration velocity accordingly.

Kirchhoff offset gathers exhibit artifacts in complex examples, which are not seen in wave equation depth-migrated images, as described in Stolk and Symes, *Kinematic artifacts in prestack depth migration*, Geophysics v. 69, p. 562 (2004). Claerbout, *Imaging the Earth's Interior* (1985), which is incorporated by reference herein, devised the zero-time/zero-offset prestack imaging condition which forms the basis of most wave equation MVA techniques. Subsurface offset gathers can be converted to angle gathers by slant-stacking as described by Prucha et al, *Angle-domain common image gathers by wave-equation migration,* 69th Annual International Meeting, SEG, Expanded Abstracts, p. 824 (1999) and by Sava and Fomel, *Angle-domain common-image gathers by wavefield continuation methods*, Geophysics v. 68, p. 1065 (2003), and have been used for MVA, as described by Clapp, *Incorporating geologic information into reflection tomography*, Geophysics v. 69, p. 533, (2004) and by Sava, *Migration and velocity analysis by wavefield extrapolation*, Ph.D. thesis, Stanford University (2004). However, the slant stack may itself introduce spurious artifacts. Shen et al., *Differential semblance velocity analysis by wave-equation migration*, SEG Expanded Abstracts, p. 2132 (2003) describe a velocity update method which uses misfocusing in subsurface offset directly.

Another class of MVA methods uses the other wave equation prestack focusing criterion—misfocusing in time—to quantify velocity errors. As described by MacKay and Abma, *Imaging and velocity estimation with depth-focusing analysis*, Geophysics v. 57, p. 1608 (1992), which is incorporated by reference herein, time-shift gathers can be constructed by phase-shifting source and receiver wave fields in shot record migration. While time-shift gathers can be converted to angle gathers, as described by Sava and Fomel, *Time-shift imaging condition in seismic migration*, Geophysics, v. 71, p. 209 (2006), which is incorporated by reference herein, MacKay and Abma measured the depth corresponding to best focusing and invoked a relationship attributed to Faye and Jeannot, *Prestack migration velocities from focusing analysis*, SEG Expanded Abstracts, p. 438 (1986), which is incorporated by reference herein, to relate the measured depth error to a velocity perturbation. The technique has small reflector dip and small offset assumptions. Audebert and Diet, *Migrated focus panels: Focusing analysis reconciled with prestack depth migration*, SEG Expanded Abstracts, p. 961 (1992), which is

incorporated by reference herein, outline an approach to partially overcome these limitations.

In the 1990's, one of the inventors, Dr. Higginbotham, developed a method of computing the propagation velocity of seismic waves in earth. The method assumed a migration velocity, generated time shift gathers using a shot record downward continuation depth migration and the time-shift imaging condition, and converted the time shift gathers to semblance gathers. The energy peaks on the semblance gathers corresponded to the amount of misfocusing in time. The magnitude of the misfocusing in time was used to update the migration velocity. The method incorrectly assumed that a time shift corresponded to zero offset travel time. The method computed inaccurate values of the propagation velocity of seismic waves in the presence of reflector dip and source-receiver offset, and it was not understood how to increase its accuracy.

SUMMARY OF THE INVENTION

The invention solves the problem of finding an accurate measure of the true propagation velocity of seismic waves in the earth, which is a condition for obtaining an accurate image of subsurface geology that can be used to prospect for oil and gas deposits.

The invention provides methods and computer-readable medium of computing the propagation velocity of seismic waves in earth, comprising: providing an estimate of the propagation velocity; generating a time shift gather using a depth migration at a plurality of locations of the earth; converting each of the time shift gathers to a semblance gather; transforming each semblance gather into a velocity gather whose energy peaks represent a root-mean-square average of the propagation velocity along the forward and backward path between earth's surface and a point of the subsurface geology; and converting the energy peaks to the propagation velocity.

The invention also provides a method of computing a propagation velocity of seismic waves in earth, comprising: providing an estimate of the propagation velocity; generating a time shift gather using the depth migration at a plurality of locations of the earth; transforming each time shift gather into a velocity gather whose energy peaks represent a root-mean-square average of the propagation velocity along the forward and backward path between earth's surface and a point of the subsurface geology, and converting the energy peaks to the propagation velocity.

The invention relates to a velocity estimation technique which uses the time-shift imaging condition for wave equation prestack depth migration. The migration time-shift parameter is converted to a perturbation in RMS velocity, which can be converted to interval velocity. The invention can resolve velocity errors in the presence of subsurface complexity that would hamper velocity analysis with surface data. Moreover, it has no dip or offset limitations for constant velocity and weak dip limitations for varying velocity.

BRIEF DESCRIPTION OF THE FIGURES

FIG. **1** illustrates a computer for implementing the methods of the invention.

FIGS. **2A-2C** illustrate downward continuation migration when the correct migration velocity is used.

FIGS. **3A-3C** illustrate downward continuation migration when an incorrect migration velocity is used.

FIGS. **4A-4B** illustrate construction of a time-shift gather when an incorrect migration velocity is used.

FIG. **5** illustrates a seismic survey geometry and a shot image aperture.

FIG. **6** illustrates a method of downward continuation shot record migration.

FIG. **7** illustrates a method of construction of a time-shift gather.

FIGS. **8A-8C** illustrate a method of flattening or retardation of a time-shift gather.

FIG. **9** illustrates counting the shots contributing to a time-shift gather.

FIG. **10** illustrates a method of semblance computation.

FIG. **11** illustrates a method of wave equation migration velocity focusing analysis.

FIGS. **12A-12C** illustrate selecting by user input energy peaks on velocity gathers.

FIG. **13** illustrates automatically selecting of energy peaks on velocity gathers.

FIG. **14** illustrates a method of updating the migration velocity.

FIG. **15** illustrates a time-shift gather based on synthetic data.

FIGS. **16A-16C** illustrate velocity gathers with varying amounts of velocity error.

FIGS. **17A-17C** illustrate migration results with varying velocity errors.

FIGS. **18A-18C** illustrate a comparison of velocity models used in a feasibility test.

DETAILED DESCRIPTION OF THE PREFERRED EMBODIMENTS

The following description includes the best mode of carrying out the invention. The detailed description is made for the purpose of illustrating the general principles of the invention and should not be taken in a limiting sense. The scope of the invention is determined by reference to the claims. Each part (or step) is assigned its own part (or step) number throughout the specification and drawings.

FIG. **1** illustrates a cluster of hosts that can execute the methods in software as described below. Each host is a computer that can communicate with data storage subsystems **11** and **26** (e.g., a disk array or solid state memory) and with each other. Hennessy and Patterson, *Computer Architecture: A Quantitative Approach* (2006), and Patterson and Hennessy, *Computer organization and Design: The Hardware/Software Interface* (2007) describe computer hardware and software, storage systems, caching, and networks and are incorporated by reference.

As shown in FIG. **1**, a first host **18**, which is representative of the second host **19** through Nth host **20**, includes a motherboard with a CPU-memory bus **14** that communicates with dual processors **13** and **16**. The processor used is not essential to the invention and could be any suitable processor such as the Intel Pentium processor. A processor could be any suitable general purpose processor running software, an ASIC dedicated to perform the operations described herein or a field programmable gate array (FPGA). Also, one could implement the invention using a single processor in each host or more than two processors to meet various performance requirements. The arrangement of the processors is not essential to the invention. Data is defined as including user data, instructions, and metadata. The processor reads and writes data to memory **15** and/or data storage subsystem **11** and **26**. Each host includes a bus adapter **22** between the CPU-memory bus **14** and an interface bus **24**.

A seismic survey may contain hundreds of thousands of shot gathers resulting in a data set greater than one terabyte.

Our method of computing the propagation velocity (described below) can be implemented on one host having a processor, but preferably uses many hosts each with a plurality of processors to image the shot gathers in parallel. In an embodiment, the method is implemented on at least 20 hosts, each having four processors. In the embodiment, each processor on each slave host communicates with a processor on a master host with data flowing between the master and the slave hosts throughout the computation. Data used by our method is usually stored locally on the slave hosts. After the work on each slave host completes, its portion of the output is summed into a single file on the master host. The SeisPak® software owned by Chevron Corporation, San Ramon, Calif. and licensed to the applicants is a suitable software environment for implementing the method described below. Seis-Pak® uses the open source Parallel Virtual Machine (PVM) software package distributed by Oak Ridge National Laboratory, Oak Ridge, Tenn. to implement the parallel computations described above.

Each host runs an operating system such as Linux, UNIX, a Windows OS, or another suitable operating system. Tanenbaum, *Modern Operating Systems* (2008) describes operating systems in detail and is hereby incorporated by reference. Bovet and Cesati, *Understanding the Linux Kernel* (2005), and Bach, *Design of the Unix Operating System* (1986) describe operating systems in detail and are incorporated by reference herein.

FIG. 1 shows that the first host 18 includes a CPU-memory bus 14 that communicates with the processors 13 and 16 and a memory 15 which is connected to memory cache 10. The first host 18 communicates through the network adapter 17 over a link 28 with a computer network 31 with other hosts. Similarly, the second host 19 communicates over link 29 with the computer network 31, and the Nth host 20 communicates over link 30 with the computer network 31. In sum, the hosts 18, 19 and 20 communicate with each other and with the computer network 31. The link 27, the link 29, the link 30, and the computer network 31 can be implemented using a suitable known bus, SAN, LAN, or WAN technology such as Fibre Channel, SCSI, InfiniBand, or Ethernet, and the technology implemented is not essential to the invention. See Kembel, The FibreChannel Consultant, *A Comprehensive Introduction* (1998), Kembel, The FibreChannel Consultant, *Arbitrated Loop* (1996-1997) The FibreChannel Consultant, *Fibre Channel Switched Fabric* (2001), Clark, *Designing Storage Area Networks* (2003), Clark, *IP SANs: A Guide to iSCSI, iFCP, and FCIP Protocols for Storage Area Networks* (2002) and Clark, *Designing Storage Area Networks* (1999), which are incorporated by reference herein.

FIGS. 2A-2C and FIGS. 3A-3C illustrate methods of applying downward continuation for prestack depth migration with the zero time lag correlation imaging condition. FIGS. 2A-2C illustrate the method when the migration velocity equals the true propagation velocity.

In FIG. 2A, dipping geologic interface 50 produces a seismic reflection which is recorded as a seismic trace (FIG. 2B) at the depth z=0, which can be on or below earth's surface. The voltage of the receiver plots the seismic energy as a function of time t. A simulated source trace 52 is also shown in FIG. 2B. The energy peak of the simulated source trace 52 will lie at t=0 when z=0. The source generating a seismic wave and the receiver which generates the voltage indicative of the wave's reflected energy records its travel time at two-dimensional surface coordinate vectors s=[sx, sy] and g=[gx, gy] as shown in FIG. 5. The simulated source trace 52 is assumed to lie at the position s. The vector connecting the source position s and the receiver position g, referred to as the

"offset" vector, can be oriented at an arbitrary azimuth with respect to the (x, y) axis as shown in FIG. 5.

As shown in FIG. 2B, the simulated source trace 52 and the recorded trace 54 are downward continued in depth to some depth $z=z_a>0$, producing traces 56 and 58. The energy peak of the downward continued simulated source trace 56 is moved to a later time. The energy peak of the downward continued recorded trace 58 is moved to an earlier time. At the focusing depth z_f the energy peak of the downward continued simulated source trace 60 and the energy peak of the downward continued recorded trace 62 are coincident in time. Because the migration velocity corresponds to the true propagation velocity, the focusing depth, z_f, is the same as the true reflector depth, z_r.

FIG. 2C illustrates applying the zero time lag imaging condition 64 to create a depth image trace 66. To form an image at depth z=0, the value corresponding to the dot product of the traces 52 and 54 is placed on the depth image trace at depth z=0. The image at $z=z_a$ is formed by applying the imaging condition 64 to the traces 56 and 58. The image at $z=z_r$ is formed by applying the imaging condition 64 to the traces 60 and 62. Because the migration velocity equals the true propagation velocity, the energy peak of the image trace reaches a maximum at the true reflector depth $z=z_r$.

FIGS. 3A-3C illustrate the same method depicted in FIGS. 2A-2C, but in the situation where the migration velocity is faster than the true propagation velocity.

As shown in FIG. 3A, the migration velocity is too fast, which causes the focusing depth z_f to be greater than the true reflector depth z_r.

FIG. 3B illustrates the same method depicted in FIG. 2B. The downward continuation of a simulated source trace 72 produces a trace 76 at z_a and a trace 80 at z_r. The downward continuation of a recorded trace 74 produces a trace 78 at z_a and a trace 82 at z_r. Because the migration velocity is too fast, the energy peaks of the trace 80 and trace 82 are not time-coincident but separated by time Δt.

FIG. 3C illustrates the same method depicted in FIG. 2C. The zero time lag correlation imaging condition 64 is applied at each depth. Because the migration velocity is too fast, the energy peak of the depth image trace 84 is deeper than the true reflection depth z_r.

FIGS. 4A-4C illustrate applying the time-shift imaging condition to the downward continued traces 80 and 82 (FIG. 4A) when the migration velocity is too slow.

As shown in FIG. 4B, an ensemble of shifted traces 90 is generated by applying opposing time shifts τ ranging from τ_{min} to τ_{max} to the trace pair 80 and 82 shown in FIG. 4A. The zero time lag correlation imaging condition 64 is applied to each of the shifted trace pairs. In this case, at τ>0 the energy peaks of the traces in the trace pairs are time coincident.

FIG. 4C shows a time-shift gather 92. The shaded row of the time-shift gather at $z=z_r$ is filled by applying the time-shift imaging condition 64 to each trace pair in the ensemble of shifted traces 90 shown in FIG. 4B. The time-shift gather is filled for other depth levels generating a slanting seismic event in the (z, τ) plane for each reflector. For a reflector, the energy of the slanting seismic event will be largest at the focusing depth z_f. Corresponding to the focusing depth z_f is a focusing time shift τ_f. Because the migration velocity is incorrect, the focusing time shift τ_f is not zero.

The magnitude of the focusing time shift τ_f can be used in an embodiment to approximate the velocity error which caused the focusing time shift to deviate from zero. The estimated velocity error is then used to update the migration velocity to better approximate the propagation velocity.

FIG. 5 illustrates the geometry of a seismic survey and a shot record migration aperture. The seismic survey includes a collection of shot gathers. Each shot gather consists of a source (or shot). The ith shot is located at position vector [sx_i, sy_i]. A collection of receivers records seismic reflections from each source. Three such receivers corresponding to the ith shot are shown at [$gx_{i,1}$, $gy_{i,1}$], [$gx_{i,2}$, $gy_{i,2}$], and [$gx_{i,j}$, $gy_{i,j}$], where the index j represents the jth receiver belonging to the ith shot. A polygon 132 contains all the receivers corresponding to the ith shot. Although shown as a rectangle, the polygon is generally irregular. A polygon 128 contains all the sources and receivers. The polygon is typically irregular in shape due to constraints such as oilfield equipment and irregularities in land ownership. The shot record migration produces an independent seismic image for each shot gather.

To reduce computational time, a shot image aperture 130 can be defined for each shot gather. The shot image aperture 130 is usually a rectangle for simple implementation. Whatever its geometric shape, the shot image aperture 130 should contain the source and all receivers in the shot gather, and enough "padding" on the edges to image seismic energy reflecting from dipping reflectors. The master image extent 126 contains all shot image apertures and is generally rectangular for simple implementation.

The location of a time-shift gather in general is denoted by (x_n, y_n). Three such locations are shown at (x_1, y_1), (x_2, y_2), and (x_n, y_n). Two of the three time-shift gather locations are contained in the shot image aperture 130 of the ith shot. Energy from the ith shot image will only contribute to time-shift gather locations contained in the shot image aperture 130. The spacing density and regularity of the time-shift gathers is flexible but can be specified on a regular grid for simplicity.

FIG. 6 illustrates a method of shot record migration to generate time-shift gathers as implemented in software executable by the host. A discrete Fourier transform is applied to the time axis of every trace in the collection of input shot gathers. The shot record migration method includes three nested loops: over all frequencies, over all shot gathers, and over all depths. It is known that summation of the frequency components of a Fourier-transformed signal is equivalent to extraction of the original signal at zero time. The zero lag correlation imaging condition is applied in this manner for efficient computation. Each shot gather is imaged independently with a pre-defined aperture then inserted and summed into the master image as shown in FIG. 5. For each frequency and each shot, the image is formed by downward continuation from the minimum depth to the maximum depth.

As shown in FIG. 6, at step 138 the user inputs the parameters for the frequency axis, the output image's depth axis, and the number of shot gathers N_{shots} in the host. It is simplest to parameterize the axes by the minimum value, the spacing between samples, the maximum value, and an integer index. The minimum frequency is ω_{min}, the spacing between adjacent frequencies is $\Delta\omega$, and the maximum frequency is ω_{max}. Similarly, the minimum depth is z_{min}, the spacing between adjacent depths is Δz, and the maximum depth is z_{max}. Implementations using irregular sampling in depth may yield a significant performance advantage, because seismic velocities generally increase with depth and high frequencies in the data are attenuated allowing less frequent sampling as the seismic waves propagate into the earth.

At step 140, the method initializes the frequency loop index j to 0. At step 142 the method computes the current frequency by the linear relation $\omega = j*\Delta\omega + \omega_{min}$. At step 144, the method initializes the shot gather index i to 0. At step 146, the method reads the location of the ith source, (sx_i, sy_i) from

the trace header of any trace in the current shot gather. Those skilled in the art are familiar with the concept of trace headers. The SEG-Y format is one example of a data format which uses trace headers. At step 146, the method also defines the spatial extent of the shot image aperture 130 relative to (sx_i, sy_i). At step 148, the method reads a Fourier-transformed synthetic source function for the current frequency. Because the source function depends on three variables, extraction of one frequency value is a "frequency slice" from the three-dimensional source function cube. Although this synthetic source function may have finite spatial extent, it can be implemented as a point source at (sx_i, sy_i), and is defined either as a "spike" at time=0 or as a more complicated function in time, which reproduces the behavior of the actual source function of the shot. At step 152, the method initializes the source wave field S, which is a two-dimensional array corresponding to the shot image aperture, by interpolating the synthetic source function into the appropriate location on S. At step 150, the method reads a frequency slice from the current Fourier-transformed shot gather. At step 154, the method initializes the receiver wave field R as it did with the source wave field at step 152 by interpolating the shot gather frequency slice read at step 150 into the appropriate location. The receiver wave field R is also a two-dimensional array with the same size as source wave field S. The initialization of receiver wave field R and source wave field S is assumed to happen at depth z=0, where the sources and receivers are assumed to be located. Generalization of the algorithm to a non-flat acquisition datum is possible, as described in Higginbotham, *Directional depth migration*, Geophysics, v. 50, p. 1784 (1985), which is incorporated by reference herein.

At step 156, the method executes a loop over depth that begins by initializing the depth index k to 0. At step 158, the method computes the kth depth by the linear relation $z = k*\Delta z + z_{min}$. At steps 160 and 162, the method downward continues the source wave field S and the receiver wave field R to the next depth. For wave-equation migration, the method can execute the downward continuation by a factorization of the acoustic wave equation into a one-way wave equation, which propagates waves only down (or up) in depth as described in Claerbout, *Toward a unified theory of reflector mapping*, Geophysics v. 36, p. 467 (1971), which is incorporated by reference. This allows recursive propagation of energy from the surface (z=0) into the sub-surface (z>0).

Biondi, *3D Seismic Imaging* (2006), which is incorporated by reference, gives an overview of the implementations of the one-way wave equation. In an embodiment, the Phase Shift Plus Interpolation method described in Gazdag and Sguazzero, *Migration of seismic data by phase-shift plus interpolation*, Geophysics, v. 49, p. 124 (1984), which is incorporated by reference, is used to implement the one-way wave equation.

The method of FIG. 6 will populate the appropriate row of all time-shift gathers (See FIG. 4) at each depth by applying the time-shift imaging condition (See FIG. 7) to the source wave field S and the receiver wave field R at step 164. After application of the time-shift imaging condition, the method increments the depth index at step 166. If the maximum depth z_{max} was exceeded at step 168, the method proceeds to the next shot gather. If not, the method returns to process the next depth at step 158. The method increments the shot gather index at step 170. If the final shot has been migrated, then at step 172, the method continues to the next frequency. Otherwise, the method returns to process the next shot gather at step 146. The method increments the frequency index at step 174. If the maximum frequency, ω_{max} has been migrated, then at step 176, the method exits to write a file containing the time-

shift gathers and the amplitude-squared time shift gathers at step 178. If not, the method returns to process the next frequency at step 142.

FIG. 7 illustrates computation of a collection of time-shift gathers for a single frequency, ω, a single shot gather located at (sx_i, sy_i), and a single depth, z. The method time shifts the source wave field S and receiver wave field R from the shot record migration and correlates them for an ensemble of time shifts. For each time shift, the method extracts the time shifted trace at each time shift location within the current shot image aperture. The method enters at step 164 from the method of FIG. 6. At step 180, the method inputs the source wave field S and the receiver wave field R. As in FIG. 4, the method applies the time-shift imaging condition for a plurality of time shifts. At step 181, the method inputs the axis parameters for the time shift variable τ. It is simplest to parameterize each time shift in terms of the minimum time shift τ_{min}, the spacing between adjacent time shifts $\Delta\tau$, and the maximum time shift τ_{max}. In an alternative embodiment, the method can use irregularly-spaced time shifts. At step 182, the method initializes the time-shift index m to 0. At step 183, the method computes the current time shift τ by the linear relation $\tau=m*\Delta\tau+\tau_{min}$. At step 184, the method applies the time shift in the frequency domain via multiplication with the complex exponential $\exp(-i\omega\tau)$ to the down-going source wave field S and similarly applies time shift $\exp(i\omega\tau)$ to the up-going receiver wave field R. The method then multiplies the time shifted receiver wave field with the complex conjugate of the time shifted source wave field point-wise at each (x, y) location. The method stores the result in a temporary array A. At step 185, the method initializes the time-shift gather location index n to 0. At step 186, the method reads the current time-shift gather location (x_n, y_n). The user inputs a list of time-shift gather locations and shot image aperture dimensions at run-time. At step 187, if (x_n, y_n) lies inside the current shot image aperture (See FIG. 5), the method adds the local value of the temporary array A at (x_n, y_n) in the appropriate row of the time-shift gather at step 188, and adds the square of the local value of the temporary array A at (x_n, y_n) in the appropriate row of the amplitude-squared time-shift gather at step 189. At step 190, the method increments the time-shift gather index. If (x_n, y_n) does not lie inside the current shot image aperture, the method proceeds to step 190 without executing steps 188 and 189. If, at step 192, the method determines that the time-shift gather index exceeds the last time-shift gather index, the method proceeds to the next time shift value. Otherwise, the method returns to step 186 to process the next time-shift gather. At step 194, the method increments the time-shift index. If the method determines that the current time shift τ exceeds the maximum time-shift index τ_{max} at step 196 the method continues to step 198 at which point it returns at step 166 to the shot record migration in FIG. 6. If not, the method returns to step 183 to process the next time-shift value.

From FIG. 4, it can be seen that on a time-shift gather, the image is best focused at some τ_f, which may or may not be equal to zero. In an embodiment, the invention relates τ_f to a change in velocity. Adding this change in velocity to the migration velocity better approximates the propagation velocity which will produce more accurate images of the earth's geology. To make the focusing information on a time-shift gather more readily understood, the method converts the time-shift gathers and amplitude-squared time-shift gathers to semblance gathers.

FIGS. 8A-8C illustrate an optional and intermediate step in computing semblance gathers, referred to as "retardation" or flattening. After retardation, the slanting reflection events on

a time-shift gather and amplitude-squared time-shift gather are approximately flat as a function of time shift τ.

In FIG. 8A at step 202, the method initializes the time-shift gather index n to 0. At step 204, the method reads the current time-shift gather location (x_n, y_n) from the trace header of a time-shift gather file. At step 206, the method reads a single trace, $V_m(z)$, from the migration velocity cube at location (x_n, y_n). At step 208, the method reads the current time-shift gather. At step 210, the method reads the current amplitude-squared time-shift gather. Using the migration velocity, the method converts the depth axis of the current time-shift gather and amplitude-squared time-shift gather to time at steps 212 and 214, respectively. For each trace in the current time-shift gather, the method applies a vertical shift of magnitude τ at step 216. The method also applies a vertical shift of magnitude τ to the current amplitude-squared time-shift gather at step 218. To a first order, the method flattens each event on the time-shift gather with respect to τ about $\tau=0$. At step 220, the current retarded time-shift gather is written. At step 222, the current retarded amplitude-squared time-shift gather is written. At step 224 the time-shift gather index n is incremented. If, at step 226, the time-shift gather index exceeds the number of time-shift gathers, then the method exits at step 227. If not, the method returns to step 204 to read the next time-shift gather.

FIGS. 8B and 8C illustrate the flattening or retardation step. FIG. 8B shows a time-shift gather 228 computed when the migration velocity was faster than the propagation velocity (same as in FIG. 4). FIG. 8C shows the result of converting the depth, z, axis of time-shift gather 228 to time, t, and flattening of the slanting seismic event about $\tau=0$, to form retarded time-shift gather 229.

The number of shot record images that contribute to a time-shift gather location can be used to compute the semblance as shown in FIG. 9. As shown in FIG. 5, each shot gather image has a finite aperture which may not contain every time-shift gather location. At step 230, the method inputs the total number of shot gathers, N_{shots}, and parameters describing the size of the shot image aperture. At step 232, the method initializes the source index i to 0. At step 234, the method reads the ith source location (sx_i, sy_i) from the trace header of any trace in the current shot gather. At step 236, the method defines the shot image aperture. At step 238, the method initializes the time-shift gather index n. At step 240, the method reads the nth time-shift gather location (x_n, y_n) from the trace header of any trace in the current time-shift gather. At step 242, the method arrives at a decision block: if (x_n, y_n) is inside the shot image aperture corresponding to the source location (sx_i, sy_i), then the method increments the count of sources contributing to the current time-shift gather and writes that count in the trace header of the time-shift gather file at step 244. If (x_n, y_n) is not inside the image aperture, then the method skips step 244 and increments the time-shift gather index at step 246. If the time-shift gather index is beyond the maximum time-shift gather index, then at step 248, the method processes the next shot gather at step 250. If not, the method processes the next time-shift gather at step 240. The method next increments the shot gather index at step 250. If, at step 252, the shot gather index is beyond the maximum number of shot gathers N_{shots}, the method terminates at step 254. If not, the method returns to step 234 to process the next shot gather.

The semblance computation is illustrated in FIG. 10. At step 262, the method initializes the time-shift gather index n to 0. At step 264, the method begins to process the nth semblance gather. At steps 266 and 268, respectively, the method reads the current retarded time shift gather and retarded

11

amplitude-squared time-shift gather and stores the two-dimensional arrays, T_n and Q_n. At step **270**, the method reads the number, N, of shot gather images contributing to the current time-shift gather (See FIG. **9**) from the trace header. At step **272**, the method computes the semblance gather using the current time-shift gather, the amplitude-squared time-shift gather, and the source count. Each sample of the two-dimensional semblance gather, S_n (t, τ) is filled according to the following relation:

$$S_n(t, \tau) = \frac{T_n(t, \tau)^2}{N \cdot Q_n(t, \tau)}, \tag{1}$$

where $T_n(t, \tau)$ corresponds to a sample from the current retarded time-shift gather and $Q_n(t, \tau)$ corresponds to a sample from the current retarded amplitude-squared time-shift gather. The computed semblance gather S_n is everywhere positive with a maximum at the point of best focusing, (t_f, τ_f).

A semblance gather **341** is shown in FIG. **12C**. The energy peak **342** has a maximum at the same (t, τ) as the corresponding retarded time-shift gather **229** as shown in FIG. **8C**.

At step **274** in FIG. **10**, the method increments the time-shift gather index. If, at step **276**, the time-shift gather index is greater than the total number of time-shift gathers, the method writes a file of semblance gathers at step **278**. If not, the method computes the next semblance gather at step **264**. The method exits at step **280**.

The semblance computation of equation (1) represents only one embodiment for facilitating the interpretation of energy peaks on the time-shift gathers. In alternative embodiments, other forms of semblance may be computed. For example, MacKay and Abma, *Imaging and velocity estimation with depth-focusing analysis*, Geophysics, v. 57, p. 1608 (1992), which is incorporated by reference, describe using the envelope function, which may be used in our invention to compute other forms of coherence rather than semblance. The method can utilize the energy peaks directly on time-shift gathers without using any coherence calculation. Additionally, the method can compute the semblance in depth first then convert to time and apply the retardation to the semblance. The order in which this is done is not essential to the invention. It is also possible for the method to perform the optional retardation step after applying a semblance measure.

In an embodiment, the invention transforms a time-shift parameter, τ to a change in velocity. The physical basis of this transformation is the relation of the time shift parameter as shown in FIG. **3B**. Δt is the amount of time separating the energy peaks on a downward continued data trace and downward continued simulated source trace at depth z_r. Δt represents the travel time of a reflection event from source position s_r to the focusing depth z_f and back to the receiver position g_r. When the migration velocity is correct, Δt is zero and the change in velocity will be zero.

Levin, *Apparent velocity from dipping interface reflections*, Geophysics 36, p. 510 (1971), which is incorporated by reference herein, gives an equation ("Levin's equation") that expresses the travel time of a seismic event from a dipping reflector in terms of the "zero-offset travel time" t_0, velocity c, dip angle θ, and "half offset" h:

$$c^2 t^2 = c^2 t_0^2 + 4h^2 \cos^2 \theta. \tag{2}$$

An embodiment of the invention uses Levin's equation (2) as a starting point in the derivation of equations (14), (17), and (18), which are used to implement the method. That derivation follows below.

12

The present invention understands that in the course of shot record migration the shot gather and the simulated source trace are both downward continued to some depth Z using the migration velocity. In an embodiment, the method interprets the time t as the travel time through a "replacement overburden" having a velocity with characteristics that allow use of Levin's equation from earth's surface down to depth Z. The method relates depth Z to t_0 exactly for the constant velocity case even for dipping events. When the velocity is represented as a RMS velocity then the relation of Z to t_0 is exact for flat events and approximate for dipping events. Since the half offset h, the zero offset time t_0, and even the exact velocity, are not easily available during shot record downward continuation, the method eliminates these variables from equation (2) in favor of known quantities such as the migration velocity and travel time t.

Define Z as the vertical depth to the reflection point when h=0. Then Levin's equation (2) can be rewritten in terms of Z:

$$c^2 t^2 = \frac{4Z^2}{\cos^2 \theta} + 4h^2 \cos^2 \theta. \tag{3}$$

The method holds t, θ, and h constant and perturbs the velocity in equation (3), leading to a perturbed depth. The method defines the perturbed velocity v(t) and the perturbed depth Z' and rewrite equation (3):

$$v(t)^2 t^2 = \frac{4Z'^2}{\cos^2 \theta} + 4h^2 \cos^2 \theta. \tag{4}$$

The method subtracts equation (3) from (4) to derive a relationship between a perturbation in velocity $\Delta v(t)$ and a perturbation in depth Δz:

$$\Delta v(t) = \frac{\overline{Z}}{\overline{v}} \frac{4\Delta z}{t^2 \cos^2 \theta}, \tag{5}$$

where

$$\Delta v(t) \equiv v(t) - c; \ \Delta Z \equiv Z' - Z; \ \frac{\overline{Z}}{\overline{v}} = \frac{Z + \Delta Z/2}{c + \Delta v(t)/2}. \tag{6}$$

The method evaluates equation (3) at h=0, then relates ΔZ to a perturbation in zero offset travel time, Δt_0:

$$\Delta Z = \Delta t_0 \frac{c}{2} \cos \theta. \tag{7}$$

The method also manipulates equation (2) to relate perturbations in zero offset travel time Δt_0, to perturbations in non-zero offset travel time Δt. The method perturbs t_0 and t and algebraically rearranges equation (2) to obtain:

$$2t \Delta t \left(1 + \frac{\Delta t}{2t}\right) = 2t_0 \Delta t_0 \left(1 + \frac{\Delta t_0}{2t_0}\right). \tag{8}$$

Starting with equation (4), the method inserts the relation for average depth-to-velocity ratio from equation (6) and then uses equation (7) to replace the ΔZ terms with Δt_0 terms to obtain:

$$\Delta v(t) = \frac{ct_0 \Delta t_0}{t^2}\left(1 + \frac{\Delta t_0}{2t_0}\right)\left(1 + \frac{\Delta v(t)}{2c}\right)^{-1}. \tag{9}$$

The method recognizes a term that looks like the right-hand side of equation (8) in equation (9), and eliminates t_0 from equation (9) to obtain:

$$\Delta v(t) = \frac{c\Delta t}{t}\left(1 + \frac{\Delta t}{2t}\right)\left(1 + \frac{\Delta v(t)}{2c}\right)^{-1}. \tag{10}$$

The method further algebraically manipulates the last component of equation (10) to obtain:

$$\left(1 + \frac{\Delta v(t)}{2c}\right)^{-1} = \left(1 - \frac{\Delta v(t)}{v(t)}\right)\left(1 - \frac{\Delta v(t)}{2v(t)}\right)^{-1}. \tag{11}$$

The method also uses the fact that:

$$c = v(t)\left(1 - \frac{\Delta v(t)}{v(t)}\right). \tag{12}$$

The method uses relations (11) and (12), plus algebraic manipulations to modify equation (10) into the following relationship between residual travel time, Δt, and change in RMS velocity, $\Delta v(t)$:

$$\frac{\Delta t}{t} = -1 + \sqrt{1 + \frac{2\frac{\Delta v(t)}{v(t)}\left(1 - \frac{\Delta v(t)}{2v(t)}\right)}{\left(1 - \frac{\Delta v(t)}{v(t)}\right)^2}}, \tag{13}$$

Finally, the method associates Δt in equation (13) with the migration time shift parameter τ to obtain a relationship between $\Delta v(t)$ and τ:

$$\frac{\tau}{t} = -1 + \sqrt{1 + \frac{2\frac{\Delta v(t)}{v(t)}\left(1 - \frac{\Delta v(t)}{2v(t)}\right)}{\left(1 - \frac{\Delta v(t)}{v(t)}\right)^2}}, \tag{14}$$

A feature of the invention is the independence of equation (14) from reflector dip and offset. Further, equation (14) is exact in the case of constant velocity and arbitrary reflector dip, and also exact in the case of depth variable velocity and flat reflectors.

The method simplifies equation (14) by defining relative velocity and time shifts α and β:

$$\alpha \equiv \frac{\Delta v(t)}{v(t)}; \tag{15}$$

-continued

$$\beta \equiv \frac{\tau}{t}.$$

The method uses relations (15) to recast equation (14) as a quadratic equation in α and β. After common algebraic rearrangements of equation (15), the method obtains:

$$\frac{\beta^2}{2} + \beta - \frac{\alpha\left(1 - \frac{\alpha}{2}\right)}{(1 - \alpha)^2} = 0. \tag{16}$$

The method solves quadratic equation (16), expands the square root to three terms, and keeps only terms of order α^2, to obtain an approximation to equation (14):

$$\frac{\tau}{t} = \frac{\Delta v(t)}{v(t)}\left(1 + \frac{\Delta v(t)}{v(t)}\right). \tag{17}$$

Equation (17) is quite accurate. For a relative velocity perturbation of 10% ($\alpha = 0.1$), the correct result is $\beta = 0.111$ 1 ..., while equation (17) yields a result of $\beta = 0.11$, implying an error of only 0.1%.

Another, less accurate, approximation to equation (14) is applicable when $\Delta v(t)/v(t) \ll 1$:

$$\frac{\Delta v(t)}{v(t)} \approx \frac{\tau}{t}. \tag{18}$$

The analysis above can be repeated for depth-variable velocity. The method assumes that the reflector depth is controlled by the average velocity and repeats the analysis above, yielding a result similar to equations (14), (17), and (18), except that v(t) is replaced with RMS velocity.

The computer implemented methods of equations (14), (17), and (18) are shown in FIG. 11. At step 290, the method inputs the axis parameters for the Δv axis: the minimum value, Δv_{min}, the increment between adjacent samples, $\Delta(\Delta v)$, and the maximum value, Δv_{max}. At step 292, the method initializes the semblance gather index n. At step 294, the method reads the nth semblance gather location, (x_n, y_n) from the trace header of any trace in the semblance gather. At step 295, the method reads the current semblance gather into a two-dimensional array, $S_n(t, \tau)$. At step 296, the method reads the trace of the migration velocity at (x_n, y_n) into a one dimensional array. At step 298, the method converts the depth axis of the velocity to time. At step 300, the method permits the user to select one of the migration velocity focusing analysis (MVFA) equations, that is equation (14), (17), or (18). The MVFA transformation represents a time-dependent stretch of the τ axis of a semblance gather to Δv.

The method loops over the output domain Δv. At step 302, the method initializes the velocity perturbation index j to 0. At step 304, the method computes the current Δv by the linear equation $\Delta v = j*\Delta(\Delta v) + \Delta v_{min}$. At step 306, the selected MVFA equation computes the value of τ corresponding to the current value of Δv. At step 308, the method computes the two grid points, τ_0 and τ_1, on the τ-axis bracketing the value of τ. The method computes the linear interpolation weights, w_0 and w_1 according to the relations $w_0 = (\tau_1 - \tau)/\Delta\tau$ and $w_1 = 1 - w_0$, where $\Delta\tau$ is the distance between adjacent τ grid points on $S_n(t, \tau)$. For each time t the method averages the values of the sem-

blance gather at the two bracketing grid points to produce one sample of the velocity gather $M_n(t, v_m(t)+\Delta v)$ at step **309**. Although the MVFA mapping of equations (14), (17), or (18) is between τ and Δv, in the mapping shown at step **309**, τ is mapped to $v+\Delta v$. The method may also define the velocity gather only in terms of Δv. At step **310**, the method increments the velocity perturbation index. If, at step **312**, the current Δv value is equal to Δv_{max}, the method proceeds to step **314**. If not, the method returns to process the next velocity perturbation at step **304**. At step **314**, the method writes the recently computed velocity gather. At step **316**, the method increments the semblance gather index. If the semblance gather index is beyond the last semblance gather index at step **318**, the method terminates at step **320**. If not, method returns to step **294** to compute the next velocity gather.

After the method converts a semblance gather to a velocity gather as described by FIG. **11**, the method maps a given energy peak on the semblance gather, (t_f, τ_f) to an energy peak on the velocity gather $(t_f, v_{rms}+\Delta v_{rms})$. FIG. **12C** shows an energy peak **342** on a semblance gather **341**. The method maps that energy peak to a corresponding energy peak **348** on the velocity gather **344** as shown in FIG. **12D**. The migration velocity **346**, $V_m(t)$ is plotted as a thick dotted line. If, as in FIG. **12D**, the migration velocity is too slow, the energy peak on the velocity gather **344** indicates that a higher velocity is needed to approximate the propagation velocity. The method defines the output velocity gather in terms of total updated velocity ($v_{rms}+\Delta v_{rms}$). The method may also define the velocity gather in terms of velocity change Δv_{rms} alone.

FIGS. **12-14** illustrate a method to update the migration velocity to approximate the true propagation velocity. FIG. **12A** illustrates that the host can display the results to human who can visually pick the energy peaks of the velocity gathers. At step **330**, the velocity gather file is input to an application which allows a user to view a velocity gather, pick individual points in (t, v_{rms}) space and save the points to a file. Many suitable software applications exist such as the GSEGYView viewer, which is available and can be downloaded from SourceForge at www.sourceforge.net. The user can loop over the desired velocity gathers as described earlier. Starting with the first velocity gather at step **332**, the method displays the current velocity gather at step **334**. At step **336**, the user selects energy maxima on the current velocity gather that correspond to the subsurface reflection events. If the user has reached the last velocity gather at step **338**, then at step **339**, the user's selection of (t, v_{rms}) is written to a file and the method terminates at step **340**.

FIGS. **12B**, **12C**, and **12D** illustrate the processing sequence from retardation of time-shift gathers to semblance gathers to picking velocities on velocity gathers. The retarded time-shift gather **229** shown in FIG. **12B** is the same as retarded time-shift gather **229** shown in FIG. **8C**. The energy peak **342** on the corresponding semblance gather **341** is shown in FIG. **12C**. FIG. **12D** shows how energy peak **342** on FIG. **12C** is mapped to an energy peak **348** on the velocity gather **344**. The migration velocity **346**, $V_m(t)$, is plotted as a thick dotted line. If the migration velocity is too slow, the energy peak **348** on the velocity gather **344** indicates that a velocity speedup is needed to better approximate the true propagation velocity. The bold "x" symbol **349** represents a single (t, v_{rms}) selection that can be made by a human interpreter as described in FIG. **12A** or by a computer as described below in FIG. **13**. The collection of all (t, v_{rms}) picks on all velocity gathers can be used to update the migration velocity.

FIG. **13** illustrates a computer implemented method that selects the energy peaks on velocity gathers. At step **350**, the method inputs the axis parameters for the velocity axis: the

minimum value v_{min}, the increment between adjacent samples Δv, and the maximum value v_{max}. The velocity gather's horizontal axis is parameterized in terms of velocity and not the velocity perturbation. Also at step **350**, the method inputs the axis parameters for the time axis, the minimum value t_{min}, the increment between adjacent samples Δt, and the maximum value t_{max}. At step **352**, the method initializes the velocity gather index n to 0. At step **354**, the method reads the current velocity gather into a two-dimensional array, the axes of which are time and velocity. At step **356**, the method initializes the time index k to 0. At step **358**, the method computes the current time t by the linear equation $t=k*\Delta t+t_{min}$. At step **360**, the method computes the velocity index m, corresponding to the maximum value of the row of the velocity gather at the current time index. At step **362**, the method computes the RMS velocity, v_{rms}, corresponding to the velocity index m by the linear equation $v_{rms}=m*\Delta v+v_{min}$. At step **364**, the method stores the current (t, v_{rms}) value corresponding to the current energy peak. At step **366**, the method increments the time index. If the time corresponding to the incremented time index exceeds t_{max} at step **368**, the method proceeds to step **370**. If not, the method returns to step **358** to process the next time value. At step **370**, the method increments the velocity gather index. If, at step **372**, the velocity gather index exceeds the maximum velocity gather index, the method proceeds to step **374**. If not, the method returns to step **354** to process the next velocity gather. At step **374**, the method writes the stored collection of (t, v_{rms}) values. At step **376**, the method exits.

FIG. **14** illustrates how the energy peaks selected by the methods of FIG. **12** or FIG. **13** can be used to update the migration velocity. At step **380**, the method inputs the energy peaks from either FIG. **12** or FIG. **13**. At step **382**, the method initializes the velocity gather index n. At step **384**, the method updates the migration velocity at the current velocity gather location. At step **386**, the method uses the (t, v_{rms}) selected at the current velocity gather location to derive an interval velocity, $v_{mig}(t)$, as a function of depth by solving the Dix equation with feasibility constraints (i.e., greater than a realistic minimum velocity and less than a realistic maximum velocity) on the value of the velocity. The Dix equation is described in C. H. Dix, *Seismic velocities from surface measurements*, Geophysics, v. 20, p. 68 (1955), which is incorporated by reference herein. At step **388**, the method increments the velocity gather index. If the method determines the last velocity gather index has been exceeded at step **390**, the method proceeds to step **392**. If not, the method returns to process the next velocity gather at step **384**. After the velocity gather locations have been processed, the method interpolates the collection of sparsely sampled interval velocity functions, $v_{mig}(t)$, at step **392** to form a fully sampled volume of updated migration velocities. At step **394**, the method applies constraints to enforce mathematical properties (i.e., continuity of the velocity and/or the first derivative) across the interpreted geologic interfaces. At step **396**, the method applies polynomial smoothing to smooth the velocity within each geologic layer defined by the user. At step **398**, the method exits. It should be noted that steps **386**, **392**, **394**, and **396** may be accomplished using the SeisPak software system, described earlier.

As noted above, velocity analysis using the invention begins with time-shift gathers, computed with a wave equation shot record depth migration algorithm. FIG. **15** illustrates an actual time-shift gather **400** taken from a synthetic dataset migrated with an incorrect velocity. The velocity was correct above a depth of 2,500 m. For the deeper reflectors, the energy peaks are shifted away from $\tau=0$ by as much as −0.15 second.

FIGS. **16-18** illustrate application of the invention to a complex 2D synthetic dataset designed to mimic geologic structures such as those found in the Belridge Field, Calif., USA. The synthetic example includes 200 m of topographic relief, a weathering layer of variable thickness, significant lateral velocity variation, and dips to 75 degrees. Shot gathers were simulated over a 10 km profile, using a pseudo-spectral acoustic wave equation solver, with frequencies up to 45 Hz. Density contrasts produce most of the reflections. After building an initial velocity model, two iterations of the method were applied to test the efficacy of the method.

FIGS. **16A-16C** show velocity gathers computed using the synthetic land dataset. The thick dotted lines show the RMS migration velocity as a function of time. In an embodiment, the method updates the migration velocity by picking the velocity peaks and converting to an interval velocity using Dix equation, as shown in FIG. **14**. The dark semblance peaks **408**, **409** represent the RMS velocity implied by the method. The velocity gather **410** shown in FIG. **16A** was computed using the initial migration velocity **412**. The semblance peaks do not overlay the migration velocity, implying that the migration velocity should be slowed down or sped up. The velocity gather **414** shown in FIG. **16B** was computed using the migration velocity **416** estimated after two iterations of the method, and it can be seen that the semblance panels overlay the migration velocity more accurately than those shown in FIG. **16A**, implying that the migration velocity is closer to the true propagation velocity. The velocity gather **418** shown in FIG. **16C** was computed using the true propagation velocity **420**. Comparing FIG. **16B** to FIG. **16C**, it is apparent that by applying two iterations of the method, the propagation velocity has been accurately estimated.

FIGS. **17A-17C** show subsets of the shot record migration images corresponding to the initial migration velocity, the migration velocity after two iterations of the method, and the true propagation velocity. As shown in FIG. **17A**, the image **430** obtained by migrating with the initial migration velocity has poor focusing of the steep dips on the left side of the anticline. As shown in FIG. **17B**, after two iterations of the method, both the fault on the right side of the image **432** and the steep dips on the left side of the image are well-imaged, as are the steep dips. As shown in FIG. **17C**, the image **434** obtained by migrating with the true propagation velocity matches the image **432** obtained by migrating with the velocity estimated by the method. Some depth errors remain, mostly due to shallow low velocity pods that were not fully inverted for as shown in FIG. **18**. However, the focusing and positioning of most events in image **432** shown on FIG. **17B** confirms that the velocity obtained by applying two iterations of the method accurately approximates the true propagation velocity.

FIGS. **18A-18C** show the initial migration velocity, the migration velocity after two iterations of the method, and the true propagation velocity. As shown in FIG. **18A**, initial migration velocity **440** is simply a single v(z) function "hung" from the base of the weathering layer. As shown in FIG. **18B**, after two iterations of the method, migration velocity **442** contains considerably more structure than the initial migration velocity. FIG. **18C** shows the true propagation velocity **444**. The estimated velocity **442** is smoother than the true velocity **444**. Also, several low velocity "pods" were not reproduced by the method. This is related to the velocity inversion scheme and parameterization of the model, rather than limitation of the invention. When justified by prior information such as well logs or geologic constraints, discontinuous velocity models can be estimated. Still, comparing the migration velocity **442** to the initial velocity **440** and the true

velocity **444**, it is apparent that two iterations of the method have reconstructed the large velocity structures, which is a key element to achieve accurate event positioning after migration.

Our invention to compute the propagation velocity can be employed for seismic imaging. The invention outputs a volume (i.e., x-y-z values) of propagation velocity that can be input to an imaging method that takes in raw seismic data that has little resemblance to earth's geological layers and transforms this data into an image displayed on the host that contains clearly identifiable geological interfaces below the surface of the earth. The method also improves the fidelity of the reflection amplitude with respect to angle of incidence on the reflector.

What is claimed:

1. A computer implemented method of determining a propagation velocity of seismic waves in earth, comprising:
   using a processor;
   using a memory holding program instructions executable by the processor to implement:
   inputting an estimate of the propagation velocity;
   generating a time shift gather using a depth migration and the propagation velocity at a plurality of locations of the earth;
   converting each of the time shift gathers to a semblance gather;
   transforming each semblance gather into a velocity gather, whose energy peaks represent a root-mean-square average of the propagation velocity along a forward and backward path between earth's surface and a point of a subsurface geology;
   converting the energy peaks to the propagation velocity; and
   storing the propagation velocity.

2. The method of claim **1**, wherein converting each of the time shift gathers to a semblance gather includes:
   (a) computing an amplitude squared time shift gather, and
   (b) counting shot images contributing to each time shift gather.

3. The method of claim **1**, wherein the step of transforming each semblance gather into a velocity gather includes associating a migration time-shift parameter, τ, with a residual travel time, Δt, from the depth migration using the estimate of the propagation velocity.

4. The method of claim **3**, wherein the migration time-shift parameter, τ, on the semblance gather relates to a root-mean-square average of the propagation velocity change, $\Delta v(t)$, along the forward and backward path between earth's surface and the point of the subsurface geology.

5. The method of claim **4**, wherein the migration time-shift parameter, τ, on the semblance gather relates to the root-mean-square average of the propagation velocity change, $\Delta v(t)$, by the following formula:

$$\frac{\tau}{t} = -1 + \sqrt{1 + \frac{2\frac{\Delta v(t)}{v(t)}\left(1 - \frac{\Delta v(t)}{2v(t)}\right)}{\left(1 - \frac{\Delta v(t)}{v(t)}\right)^2}}.$$

6. The method of claim **5**, wherein transforming each semblance gather into a velocity gather includes interpolating between the migration time-shift parameter, τ, and the root-mean-square average of the propagation velocity change, $\Delta v(t)$.

7. The method of claim **6**, further comprising selecting a maxima of each of the energy peaks on the velocity gather.

8. The method of claim **7**, further comprising updating the propagation velocity, using the selected energy maxima.

9. The method of claim **5**, wherein transforming each semblance gather into a velocity gather includes interpolating between the migration time-shift parameter, τ, and the root-mean-square average of the propagation velocity change, $\Delta v(t)$, plus the estimate of the propagation velocity.

10. The method of claim **9**, further comprising selecting a maxima of each of the energy peaks on the velocity gather.

11. The method of claim **10**, further comprising updating the propagation velocity, using the selected energy maxima.

12. The method of claim **6**, wherein selecting a maxima of each of the energy peaks is performed by a computer.

13. The method of claim **4**, wherein the migration time-shift parameter, τ, on the semblance gather relates to the root-mean-square average of the propagation velocity change, $\Delta v(t)$, by the following formula:

$$\frac{\tau}{t} \approx \frac{\Delta v(t)}{v(t)}\left(1 + \frac{\Delta v(t)}{v(t)}\right).$$

14. The method of claim **4**, wherein the migration time-shift parameter, τ, on the semblance gather relates to the root-mean-square average of the propagation velocity change, $\Delta v(t)$, by the following formula:

$$\frac{\Delta v(t)}{v(t)} \approx \frac{\tau}{t}.$$

15. A computer implemented method of determining a propagation velocity of seismic waves in earth, comprising:

providing an estimate of the propagation velocity;

generating a time shift gather using a depth migration and the propagation velocity at a plurality of locations of the earth;

transforming each time shift gather into a velocity gather, whose energy peaks represent a root-mean-square average of the propagation velocity along a forward and backward path between earth's surface and a point of a subsurface geology;

converting the energy peaks to the propagation velocity; and

storing the propagation velocity.

16. The method of claim **15**, wherein the step of transforming each time shift gather into a velocity gather includes associating a migration time-shift parameter, τ, with a residual travel time, Δt, from the depth migration using the estimate of the propagation velocity.

17. The method of claim **16**, wherein the migration time-shift parameter, τ, on the time shift gather relates to the root-mean square average of the propagation velocity change, $\Delta v(t)$.

18. The method of claim **17**, wherein the migration time-shift parameter, τ, relates to the root-mean-square average of the propagation velocity change, $\Delta v(t)$, by the following formula:

$$\frac{\tau}{t} = -1 + \sqrt{1 + \frac{2\frac{\Delta v(t)}{v(t)}\left(1 - \frac{\Delta v(t)}{2v(t)}\right)}{\left(1 - \frac{\Delta v(t)}{v(t)}\right)^2}} \,.$$

19. The method of claim **18**, wherein transforming each time shift gather into the velocity gather includes interpolating between the migration time-shift parameter, τ, and the root-mean-square average of the propagation velocity change, $\Delta v(t)$.

20. The method of claim **19**, further comprising selecting a maxima of each of the energy peaks on the velocity gather.

21. The method of claim **20**, further comprising updating the propagation velocity, using the selected energy maxima.

22. The method of claim **18**, wherein transforming each time shift gather into the velocity gather includes interpolating between the migration time-shift parameter, τ, and the root-mean-square average of the propagation velocity change, $\Delta v(t)$, plus the estimate of the propagation velocity.

23. The method of claim **22**, further comprising selecting a maxima of each of the energy peaks on the velocity gather.

24. The method of claim **23**, further comprising updating the propagation velocity, using the selected energy maxima.

25. The method of claim **23**, wherein selecting the maxima of each of the energy peaks is performed by a computer.

26. The method of claim **17**, wherein the migration time-shift parameter, τ, relates to the root-mean-square average of the propagation velocity change, $\Delta v(t)$, by the following formula:

$$\frac{\tau}{t} \approx \frac{\Delta v(t)}{v(t)}\left(1 + \frac{\Delta v(t)}{v(t)}\right).$$

27. The method of claim **17**, wherein the migration time-shift parameter, τ, relates to the root-mean-square average of the propagation velocity change, $\Delta v(t)$, by the following formula:

$$\frac{\Delta v(t)}{v(t)} \approx \frac{\tau}{t}.$$

28. A non-transitory computer-readable medium storing program instructions that cause a computer to perform steps, comprising:

inputting an estimate of a propagation velocity;

generating a time shift gather using a depth migration and the propagation velocity at a plurality of locations of the earth;

converting each of the time shift gathers to a semblance gather;

transforming each semblance gather into a velocity gather, whose energy peaks represent a root-mean-square average of the propagation velocity along a forward and backward path between earth's surface and a point of a subsurface geology;

converting the energy peaks to the propagation velocity; and

storing the propagation velocity.

29. The non-transitory computer-readable medium of claim **28**, wherein converting each of the time shift gathers to a semblance gather includes:

(a) computing an amplitude squared time shift gather, and

(b) counting shot images contributing to each time shift gather.

30. The non-transitory computer-readable medium of claim **28**, wherein the step of transforming each semblance gather into a velocity gather includes associating a migration time-shift parameter, τ, with a residual travel time, Δt, from the depth migration using the estimate of the propagation velocity.

31. The non-transitory computer-readable medium of claim **30**, wherein the migration time-shift parameter, τ, on the semblance gather relates to a root-mean-square average of the propagation velocity change, $\Delta v(t)$, along the forward and backward path between earth's surface and the point of the subsurface geology.

32. The non-transitory computer-readable medium of claim **31**, wherein the migration time-shift parameter, τ, on the semblance gather relates to the root-mean-square average of the propagation velocity change by the following formula:

$$\frac{\tau}{t} = -1 + \sqrt{1 + \frac{2\frac{\Delta v(t)}{v(t)}\left(1 - \frac{\Delta v(t)}{2v(t)}\right)}{\left(1 - \frac{\Delta v(t)}{v(t)}\right)^2}} \ .$$

33. The non-transitory computer-readable medium of claim **32**, wherein transforming each semblance gather into a velocity gather includes interpolating between the migration time-shift parameter, τ, and the root-mean-square average of the propagation velocity change, $\Delta v(t)$.

34. The non-transitory computer-readable medium of claim **33**, further comprising selecting a maxima of each of the energy peaks on the velocity gather.

35. The non-transitory computer-readable medium of claim **34**, further comprising updating the propagation velocity, using the selected energy maxima.

36. The non-transitory computer-readable medium of claim **33**, wherein selecting a maxima of each of the energy peaks is performed by a computer.

37. The non-transitory computer-readable medium of claim **32**, wherein transforming each semblance gather into a velocity gather includes interpolating between the migration time-shift parameter, τ, and the root-mean-square average of the propagation velocity change, $\Delta v(t)$, plus the estimate of the propagation velocity.

38. The non-transitory computer-readable medium of claim **37**, further comprising selecting a maxima of each of the energy peaks on the velocity gather.

39. The non-transitory computer-readable medium of claim **38**, further comprising updating the propagation velocity, using the selected energy maxima.

40. The non-transitory computer-readable medium of claim **31**, wherein the migration time-shift parameter, τ, on the semblance gather relates to the root-mean-square average of the propagation velocity change by the following formula:

$$\frac{\tau}{t} \approx \frac{\Delta v(t)}{v(t)}\left(1 + \frac{\Delta v(t)}{v(t)}\right).$$

41. The non-transitory computer-readable medium of claim **31**, wherein the migration time-shift parameter, τ, on the semblance gather relates to the root-mean-square average of the propagation velocity change by the following formula:

$$\frac{\Delta v(t)}{v(t)} \approx \frac{\tau}{t}.$$

* * * * *